

# Multiple Object Detection and Tracking in Panoramic Videos for Cycling Safety Analysis

Jingwei Guo<sup>1</sup>, Meihui Wang <sup>2</sup>, Ilya Ilyankou <sup>2</sup>, Natchapon  
Jongwiriyanurak <sup>2</sup>, Xiaowei Gao <sup>2</sup>, Nicola Christie <sup>3</sup>, and  
James Haworth <sup>2,\*</sup>

<sup>1</sup>Department of Civil, Environmental, and Geomatic Engineering, University College London  
(UCL), UK

<sup>2</sup>SpaceTimeLab, Department of Civil, Environmental, and Geomatic Engineering, University  
College London (UCL), UK

<sup>3</sup>Centre for Transport Studies, Department of Civil, Environmental, and Geomatic  
Engineering, University College London (UCL), UK

\*Corresponding author: [j.haworth@ucl.ac.uk](mailto:j.haworth@ucl.ac.uk)

## Abstract

Panoramic cycling videos can record 360° views around the cyclists. Thus, it is essential to conduct automatic road user analysis on them using computer vision models to provide data for studies on cycling safety. However, the features of panoramic data such as severe distortions, large number of small objects and boundary continuity have brought great challenges to the existing CV models, including poor performance and evaluation methods that are no longer applicable. In addition, due to the lack of data with annotations, it is not easy to re-train the models.

In response to these problems, the project proposed and implemented a three-step methodology: (1) improve the prediction performance of the pre-trained object detection models on panoramic data by projecting the original image into 4 perspective sub-images; (2) introduce supports for boundary continuity and category information into DeepSORT, a commonly used multiple object tracking model, and set an improved detection model as its detector; (3) using the tracking results, develop an application for detecting the overtaking behaviour of the surrounding vehicles.

Evaluated on the panoramic cycling dataset built by the project, the proposed methodology improves the average precision of YOLO v5m6 and Faster RCNN-FPN under any input resolution setting. In addition, it raises MOTA and IDF1 of DeepSORT by 7.6% and 9.7% respectively. When detecting the overtakes in the test videos, it achieves the F-score of 0.88.

The code is available on GitHub at [github.com/cuppp1998/360\\_object\\_tracking](https://github.com/cuppp1998/360_object_tracking) to ensure the reproducibility and further improvements of results.

# 1. Introduction

35

Cycling, as an active travel mode, has zero carbon emissions (Massink et al., 2011) and can support reductions in traffic congestion (Brunsing, 1997) while improving the health of urban residents (Wanner et al., 2012). Therefore, many local governments and transport authorities are implementing policies to encourage cycling as an alternative to car travel. However, cycling is often perceived as a dangerous activity, particularly in cities that lack high quality cycling infrastructure. In London, cycle lanes account for only 6.4% of the total road length (excluding highways) (Tait et al., 2022), meaning that cyclists often have to share lanes with motor vehicles. According to Transport for London (TfL), in 2020, despite the mode share of cyclists being only 3.4%, there were 868 killed or seriously injured (KSI) incidents involving cyclists, accounting for 28% of all such casualties in the city (Transport for London, 2021). This disproportionately high risk of incidents can reduce people’s willingness to ride (Delmelle & Delmelle, 2012), which hinders the uptake of cycling. Thus, it is necessary to take measures to improve urban cycling safety, which may include improving road infrastructure (Pucher & Buehler, 2016), implementing policies such as lower speed limits, or running public awareness campaigns like Operation Close Pass (Warwickshire Police, 2023). However, in order to gain support, these improvements must be accompanied by evidence on their effectiveness. One aspect of this is the impact on cycling safety.

Although incident data are available through hospital reports and official statistical releases, such as the UK’s STATS19, the low mode share of cycling makes it difficult to draw statistically significant conclusions at a spatially and temporally granular level. Near-miss events, in contrast, are more frequent and have provided a rich source of data for researchers in the form of naturalistic studies (Ibrahim, Haworth, Christie, Cheng & Hailes, 2021). These studies have used a range of sensors to collect data while people carry out routine activities on bikes, with the rider indicating when they experience a near-miss. Alternatively, sensors are used to collect objective data on a particular near-miss type, such as a close pass (Beck et al., 2019). To date these studies have been limited in the perspective of the near-miss that they capture. In recent years, with the rapid development of street view imagery, action/dash cameras, virtual reality (VR) and related technologies, panoramic photography is becoming widespread and mature (Im et al., 2016). Unlike traditional cameras, which can only capture content within a limited field of view, a panoramic camera can capture 180-degree views of the front and rear of the device at the same time with two fisheye lenses, and then concatenate them into one high-resolution 360° image (Hua & Ahuja, 2001). These consumer grade cameras are suitable to be mounted on helmets or handlebars to record videos of the riders’ surroundings in all directions. Importantly, the 360 view captures the relative movement of the rider and the other people recorded in the scene. For example, in an overtaking manoeuvre, a vehicle will first appear in the rear-view of the camera, before passing into the side

view (right or left depending on locality) and into the front view. Computer vision based object detection and tracking technologies have the potential to track these movements and categorise them into actions based on interpretations of the relative movements.

The emergence of deep learning has had a transformative effect on a range of machine learning tasks, especially computer vision (LeCun et al., 2015). A range of algorithms have been developed for implementing various visual tasks such as object detection (Zhao et al., 2019) and multiple object tracking (MOT) (Luo et al., 2021). However, since most of these models and the attached pre-trained weights were designed and trained for traditional images and videos, if applied directly to panoramic videos in equirectangular projection, their performance will be negatively affected (Yang et al., 2018). In addition, some models' evaluation metrics are not applicable to panoramic images. These problems exist because of the following differences between panoramic images and standard images:

- The acquisition of panoramic videos requires specific cameras. As a result, the number of available annotated panoramic datasets is much lower than that of standard cameras;
- Due to the distortions introduced by the equirectangular projection, objects near the camera may be seriously deformed, while objects far away from the camera will be small;
- Panoramic images in equirectangular projection have boundary continuity in which the contents of the left and right sides of the image are continuous (Liu et al., 2018).

To overcome these limitations, this research develops a framework for applying deep learning based computer vision models pre-trained on 'traditional' datasets to the task of object detection and tracking in panoramic videos. The methodology is applied to a case study in cycling safety analysis; the identification of overtaking manoeuvres.

The remainder of the paper is structured as follows: Following this Introduction, we discuss related work on cycling safety, computer vision and its application to panoramic data in Section 2. Section 3 describes the collection, pre-processing and annotation process of the data used in this project, and introduces their distribution. In Section 4, we introduce the methodology, and then present and analyse the results in Section 5. In Section 6 we discuss the successes and limitations of our work, and propose some future work to overcome the limitations. Finally, we present our conclusion in Section 7.

## 2. Related work

### 2.1 Challenges in Understanding Cycling Crash Risk

Urban transport networks are complex environments in which many agents (pedestrians, cyclists and other road users) interact with each other while using different types of

infrastructure. In combination, these actions and interactions within the environment 109  
contribute to crash risk. Traditionally, crash risk is assessed using historical data on 110  
crash records, such as the UK's STATS19, combined with measures of exposure such as 111  
traffic flows, which are combined in a multiple regression framework to identify risk factors 112  
(Ambros et al., 2018). Existing cycling safety studies have heavily relied on crash and 113  
conflict data from open government resources (Hels & Orozova-Bekkevold, 2007; Daniels 114  
et al., 2008; Zhang et al., 2023), questionnaires surveys (Wang et al., 2020; Useche et al., 115  
2022), and crowdsourced data reported by volunteer cyclists (Poulos et al., 2012; Fischer 116  
et al., 2020). However, these data sources are often subjective and incomplete, making it 117  
challenging to understand the underlying causes of hazards. Furthermore, due to the low 118  
mode share of cycling in many countries, records on bicycle crashes may be sparse and 119  
exposure data limited to particular locations and times, or not collected at all. 120

As a complement to traditional methods, researchers have turned to naturalistic 121  
studies to observe cyclists as they carry out their routine activities (Ibrahim, Haworth, 122  
Christie, Cheng & Hailes, 2021). Typically this involves the rider using a suite of sensors 123  
that passively collect data such as video, inertial measurement unit (IMU) and location 124  
data. Early work relied on bespoke equipment for this purpose (Johnson et al., 2010), 125  
which limited its applicability beyond the scope of the study. Subsequent studies produced 126  
sensors for particular purposes, such as detecting close passes, enabling the collection of 127  
high quality, objective data (Beck et al., 2019). Ibrahim, Haworth, Christie, Cheng 128  
& Hailes (2021) provide a review of the recent work. While bespoke equipment allows 129  
a high level of control over experimental design, the use of consumer grade equipment 130  
provides an opportunity for larger scale data collection. For example, many road users 131  
routinely use dashcams or action cameras to collect data on their journeys to protect 132  
themselves if they are involved in a crash. Recognising this, recent work, particularly in 133  
the field of autonomous vehicles, has leveraged dashcam video data for crash detection. 134  
Rocky et al. (2024) provide a review of the current state of the art. Similar methods 135  
have also been applied in cycling safety analysis. For example, using data sourced from 136  
YouTube, Ibrahim, Haworth, Christie & Cheng (2021) used a deep learning approach 137  
that harnessed the optical flow of video data to detect near misses from video streams. 138  
Harnessing this data as a form of crowdsourcing could provide a way to continuously 139  
monitor safety from the cyclist's perspective, and studies such as Rick & Bustad (2021) 140  
have made use of popular devices such as GoPro cameras. 141

The key enabling computer vision technologies for understanding the risk environment 142  
from video streams are object detection and multiple object tracking (MOT). Object 143  
detection identifies and localises objects such a vehicles and people within a video frame. 144  
Techniques such as You Only Look Once (YOLO) and Faster Residual Convolutional 145  
Neural Network (R-CNN) have been employed that achieve high accuracy in detecting 146  
different road users, such as CyDet (Masalov et al., 2018) and MoDeCla (Ojala et al., 147  
2022). MOT is a task that associates multiple objects in different frames of a video into 148

several trajectories (Jiménez-Bravo et al., 2022). MOT technologies have been widely used in the field of transport, particularly autonomous vehicles. Various modifications have been made to improve car tracking in poor light conditions, continuously track road users that are sometimes occluded in the videos and to track objects using the views from multiple cameras.

Existing object detection and MOT algorithms are trained on video from cameras with a limited field of view (FOV). This suits the data that has been collected in naturalistic cycling studies to date, which contain only front or rear facing views. However, risks may be present that cannot be captured in a single view. For example, rear-end crashes have proven to result in a high fatality rate and tailgating is a risk factor. For a comprehensive view of the risk environment, it is necessary to record video both in front of and behind the rider. This can be accomplished using separate cameras, but leads to problems of synchronisation and matching of objects between the two video streams. Furthermore, the side views of the rider are not captured, which are important in the context of certain events such as close passes and car-dooring. As an alternative, panoramic cameras capture 360° views around the user, allowing seamless tracking of interactions between the rider, the environment and other road users.

Existing CV models struggle with panoramic videos due to a lack of panoramic training data, distorted and small objects in equirectangular projections, and issues with boundary continuity. Various studies have attempted to solve these issues. Some have created panoramic datasets to train existing models, while others have applied techniques to improve model performance without retraining, but these do not fully address boundary continuity or the challenge of long objects being split across sub-windows. For MOT, the quality of object detection significantly affects tracking performance. DeepSORT is a commonly used tracker that has been adapted for panoramic data. However, it faces challenges such as object ID switching caused by boundary continuity and inaccuracies in multi-category tracking (MCT). Liu et al. (2018) proposed extending input images to mitigate boundary continuity issues, yet further improvements are needed to handle objects appearing multiple times across frame boundaries and to enhance MCT.

To address these issues, our research intends to combine and extend these approaches by adding support for boundary continuity and long objects in detection, introducing category information to reduce tracking errors, and enhancing boundary continuity implementation in DeepSORT for better multi-object tracking.

### 3. Data

In order to test the improving effect of the proposed methods on object detection and MOT on panoramic cycling videos, this project built an annotated dataset so that the

Video	Length (s)	FPS	Frames	Description	Preview
Video 1	14.0	30	420	Taken on a road	
Video 2	11.1	30	333	Taken on a bicycle path	
Video 3	12.0	30	360	Taken on a road	

Table 1: Video Clips in the Annotated Dataset

performance of different models can be easily compared. In addition, for presenting and evaluating the application results of the improved models in recognising the overtakes of the surrounding vehicles, some other video clips containing overtakes were prepared.

### 3.1 Data collection

The researcher attached a GoPro Max camera to their helmet with a metal mount to take panoramic videos while riding. To ensure the authenticity of the data collected, when and where to ride was not restricted — the researcher recorded videos as they carried out routine activities such as commuting. The only limitation was that the data collection had to be in good lighting conditions so that all the objects would be recognisable in the videos.

Since the dataset with annotations was built only for evaluating the proposed models rather than training a deep neural network from scratch, there was no requirement for a large data volume. Therefore, 3 clips were chosen from the collected videos, which are 10 to 15 seconds in length, as shown in Table 1.

To evaluate the performance of the proposed model in detecting overtaking behaviour, 3 further clips of 1 to 2 minutes taken by the researcher were selected. 54 overtakes were extracted from these videos, as shown in Table 2. To mitigate bias that may be introduced by using video from a single person in a limited range of conditions, further validation is carried out on a set of video clips filmed by 49 different cyclists, who were

Video	Length (s)	FPS	Frames	Num. Overtakes	Preview
Video 5	66.0	30	1,980	12	
Video 6	108.0	30	3,240	17	
Video 7	91.0	30	2,730	25	

Table 2: Video Clips for Evaluating the Overtaking Behaviour Detection

participants in UCL’s 100 Cyclists Project. The participants, located in London, UK, 206 used the GoPro Max camera to record their activities over a period of two weeks, and 207 were instructed to say ‘near-miss’ when experiencing a near-miss event. This dataset 208 provides a wider range of riding conditions and rider characteristics on which to test the 209 proposed method: 50 of the videos contain a single clear overtaking event lasting several 210 seconds (‘positive’ examples), and 50 do not (‘negative’). To account for diverse cycling 211 environments, selected videos were captured during daytime (78), night-time (17), and at 212 dawn or dusk (5). 24 videos featured glare from the sun and artificial lighting sources, 213 such as lampposts and headlights. While only one video was recorded in rain, a further 6 214 were recorded after recent rain and are slightly obfuscated by rain drops on the camera 215 lens. 216

### 3.2 Data Pre-processing & Annotation 217

After collecting videos and selecting relevant clips, GoPro Player (GoPro, 2021a) was 218 used to trim the clips from the original videos, which are in .360 format. The ‘Horizon 219 Levelling’ functionality was applied, which uses the gyroscope data to level the videos on 220 the horizontal axis (GoPro, 2021b), as Figure 1 shows. After that, the clips were exported 221 as 5.6k ( $5,368 \times 2,688$ ) equirectangular videos in MOV format. 222

To generate labels to evaluate object detection and MOT, the videos were annotated 223 using the Computer Vision Annotation Tool (CVAT) (OpenCV, 2019) developed by Intel. 224



Figure 1: An example of the images before (left) and after (right) turning on the ‘Horizon Levelling’ functionality

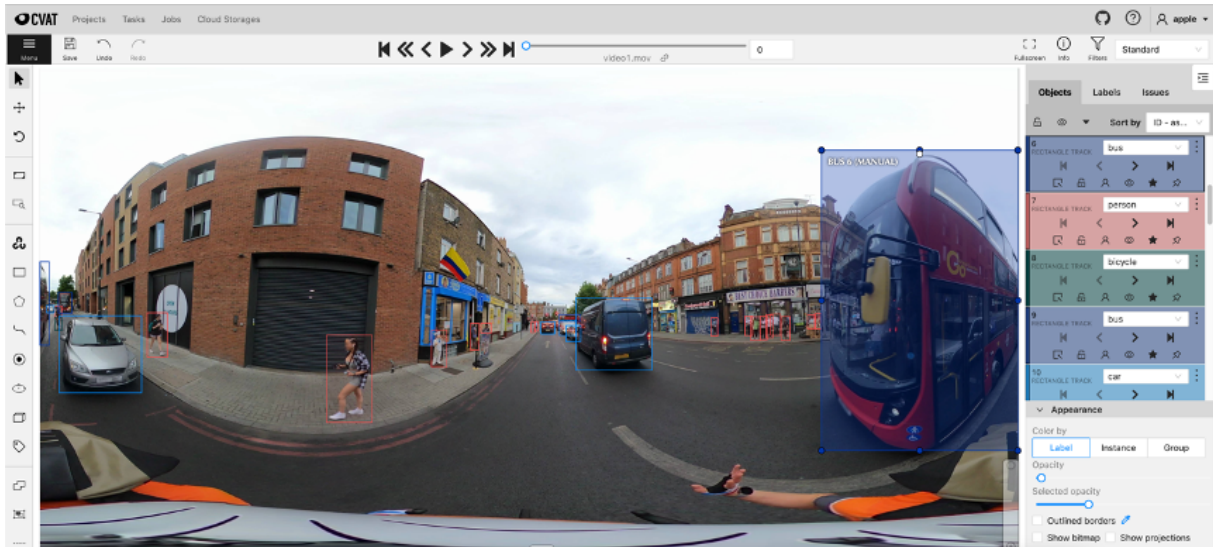


Figure 2: How objects across the boundaries were annotated in CVAT

The following 7 categories of objects were chosen for labelling, which are both relevant to 225  
cycling safety and contained in the Microsoft COCO dataset (Lin et al., 2014): person, 226  
bicycle, car, motorbike, bus, truck and traffic light. In order to output the annotations 227  
in both COCO and MOT formats, ‘tracks’ were created to associate the same objects in 228  
different image frames. 229

Following the standards of MOT format, CVAT only supports labelling each object 230  
once in each frame. Hence, objects divided into two parts due to the boundary continuity 231  
were labelled as two separate objects. For example, in Figure 2, the two parts of the bus 232  
were labelled as ‘BUS 6’ and ‘BUS 11’, respectively. 233

After the annotations were output in both COCO and MOT formats, a method was de- 234  
signed and implemented to merge these split objects in the MOT annotation files without 235  
violating the rules of MOT format (Milan et al., 2016), whose workflow is shown below: 236

After the ID modifications, FFmpeg (Mkver, 2014), an open-source command line tool, 237  
was used to split video 1, 2 and 3 into images frame by frame with the following line of com- 238  
mand: `ffmpeg -i video1.mp4 -r 30 -start_number 0 -f image2 frame_%06d.PNG`. 239  
These images are used for the evaluation of object detection models with the COCO 240  
annotation files. 241

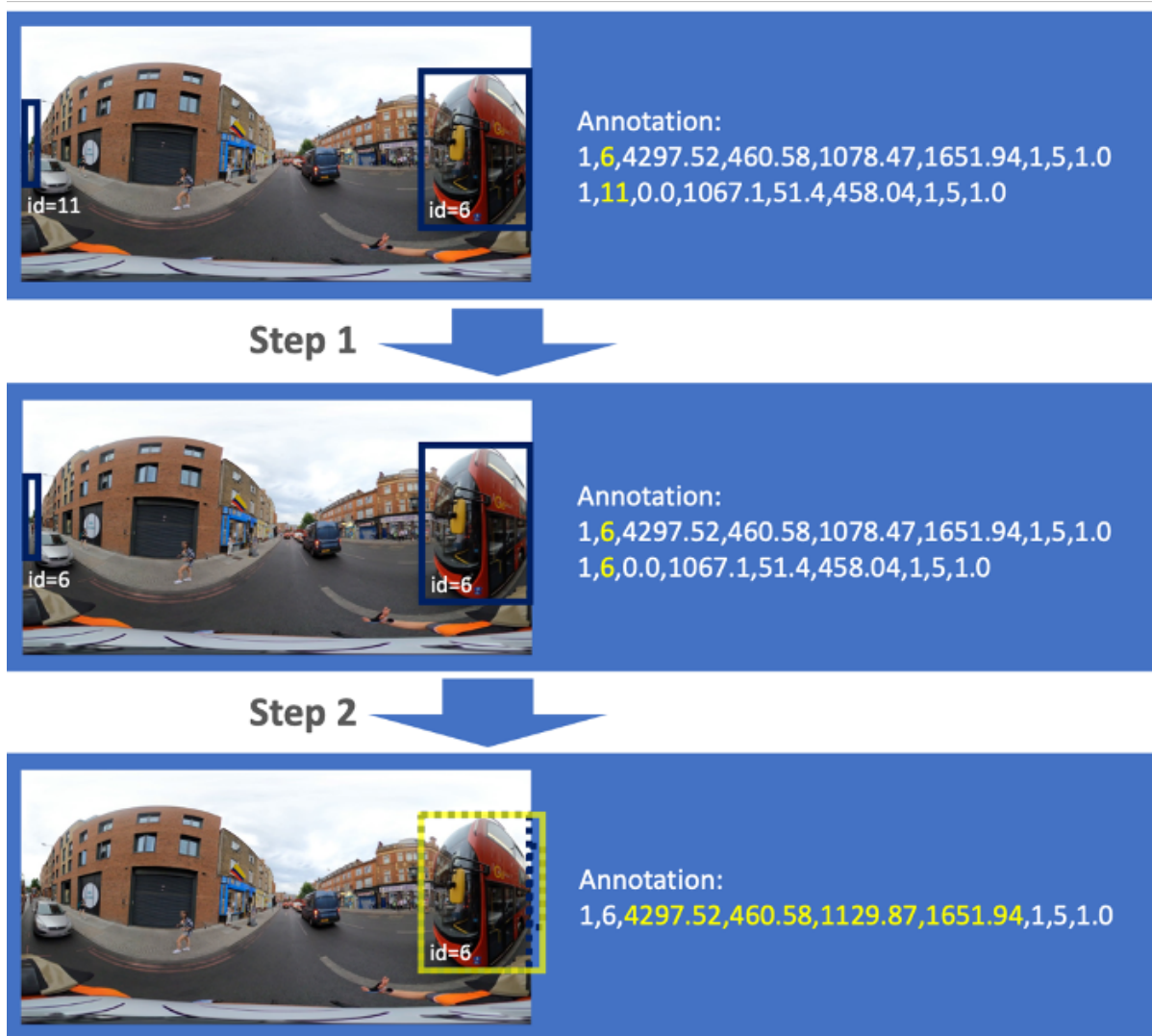


Figure 3: Workflow of merging the split objects in MOT annotation files

Video	Objects	Tracks
Video 1	9,338	75
Video 2	5,404	49
Video 3	9,712	100
Total	24,454	224

Table 3: Numbers of Objects and Tracks in the Dataset for Object Detection and MOT Evaluation

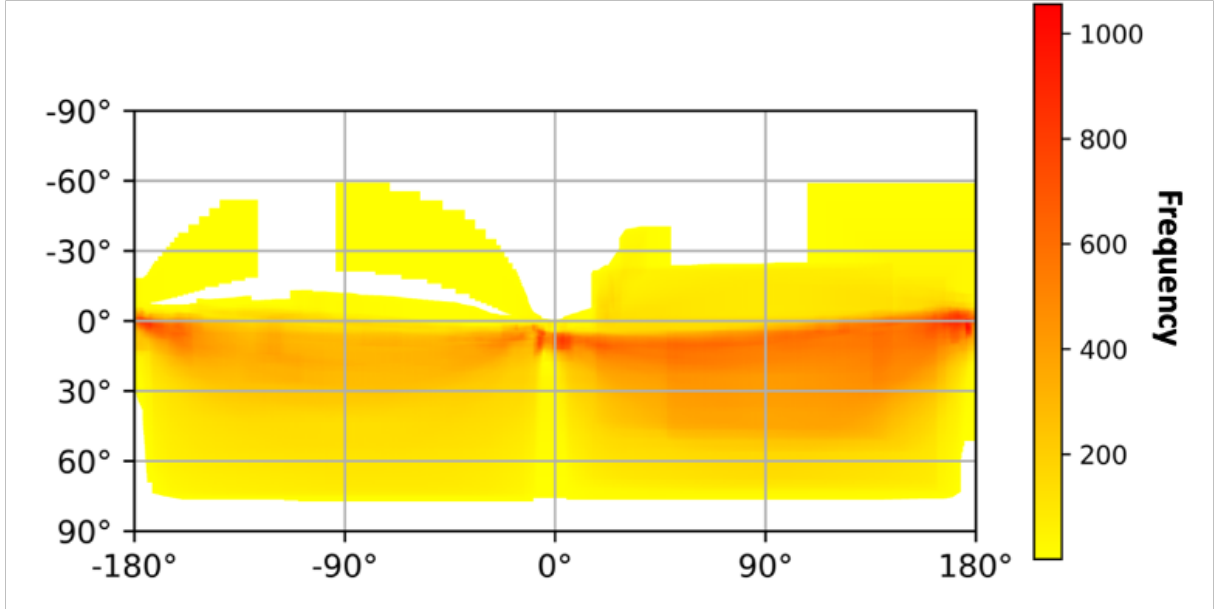


Figure 4: Position distribution of the ground truth bounding boxes in the dataset

As shown in Table 3, after pre-processing and annotation, the dataset has 24,454 242  
labelled objects and 224 labelled tracks in total. 243

### 3.3 Exploratory Data Analysis 244

In order to better design the methodologies for improving the applicability of the existing 245  
object detection and MOT models, and to better understand the corresponding evaluation 246  
results, this project conducted some exploratory analysis of the annotated dataset. 247

#### 3.3.1 Position Distribution 248

To understand where the objects of interest are located, a matrix whose size is the same 249  
as the videos ( $5,368 \times 2,688$ ) is used to count how many times each pixel is within an 250  
annotated bounding box. Then, the matrix is plotted as a heat map, as Figure 4 shows. 251  
As the top and bottom areas of an equirectangular image represent the sky and the ground 252  
respectively, almost all the objects in the dataset are distributed from  $-50^\circ$  to  $70^\circ$  of the 253  
y axes. 254

#### 3.3.2 Category Distribution 255

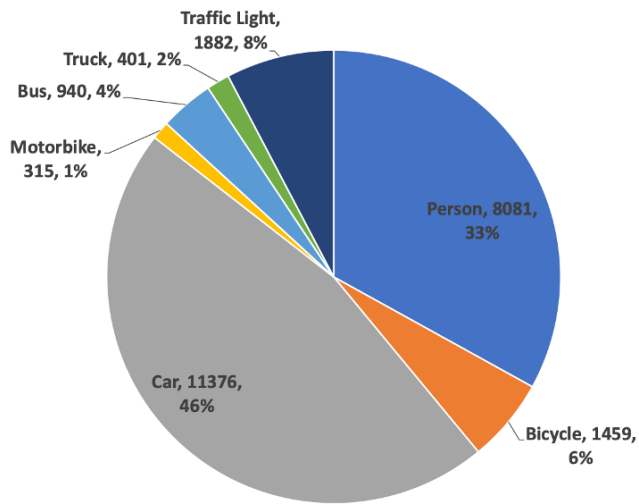


Figure 5: Category distribution of the ground truth bounding boxes in the dataset

For the purpose of knowing whether the seven categories of the labelled objects are balanced, a pie chart containing the number and proportion of the bounding boxes of each class was plotted, as shown in Figure 5. The dataset is imbalanced — the two categories with the largest quantities (car and person) account for about 80% of the total number, while motorbikes, trucks and buses, which appear less frequently in the selected videos, have less than 1,000 labelled instances.

### 3.3.3 Size Distribution

Detecting small objects is a problem for object detection models due to the small number of features they include (Li et al., 2017). Thus, it is pertinent to explore the distribution of objects of different sizes.

When classifying the bounding boxes by their area, the project did not use thresholds set by COCO, which are 322 and 962 (Lin et al., 2014) — since the resolution of the images in this test set ( $5,368 \times 2,688$ ) is much higher than that of COCO ( $640 \times 480$ ), objects should also contain more pixels. According to the ratio of the number of pixels on the short side (5.6:1), the thresholds were defined as 1282 and 3842, that is to say, objects with an area less than 1282 were classified as ‘small objects’, objects larger than 3842 were classified as ‘large objects’, while the remaining ones were classified to be ‘medium-sized’.

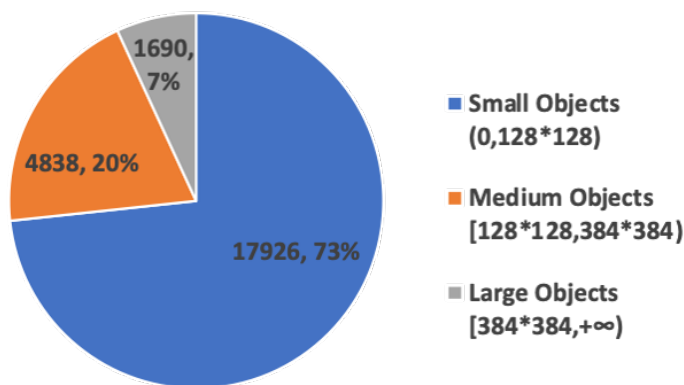


Figure 6: Size distribution of the ground truth bounding boxes in the dataset

From Figure 6, it can be seen that a large proportion of the annotated bounding boxes are small ones. Contrastingly, ‘large objects’ account for less than 10% of the annotations. Such size distribution is consistent with the characteristics of equirectangular panoramic videos summarised previously.

## 4. Methodology

In order to apply computer vision models to automated road user



Figure 7: Three steps of the methodology

behaviour analysis of panoramic cycling videos, this project designed and implemented a three-step methodology, as shown in Figure 7.

As the first step of the methodology, an approach was designed to improve the applicability of the existing pre-trained object detection models to equirectangular images. Then, in the second step, the improved models in step 1 are set as the detector of DeepSORT and its modified structure is modified according to the characteristics of panoramic videos. Finally, in step 3, a simple application was designed and developed which can automatically detect the overtaking behaviour of the surrounding vehicles in panoramic videos using the tracking results from step 2.

## 4.1 Improving Object Detection on Panoramic Images

The proposed method, shown in Figure 8, consists of the following four operations: 1) Project the equirectangular image into four sub-images of perspective projection whose distortions are less severe; 2) Implement object detection models pre-trained on the COCO dataset to identify objects in each of the sub-images; 3) Reproject the detected bounding boxes in the sub-images to the original image; 4) Since some long objects (such as the blue and red cars in Figure 8) are divided into several parts and shown in different sub-images, their bounding boxes are merged.

In the following subsections, each of these steps are explained in detail. After that, the evaluation method is introduced.

### 4.1.1 Projection Transformation from Equirectangular to Perspective

As an approach to presenting a whole sphere as a 2D image, equirectangular projection maps longitude lines and latitude circles to equally spaced vertical and horizontal lines, respectively (Snyder, 1997). In contrast, perspective projection only maps part of a sphere (within the FOV) from the centre to a tangent plane (Yang et al., 2018). Thus, essentially, the transformation from equirectangular to perspective is a projection from a sphere to a plane.

According to Lee (2021), as shown in Figure 9 (a), assuming that the perspective projection is along the  $z$ -axis, the corresponding point  $P'$  ( $X, Y, Z$ ) on the sphere of the point  $P$  ( $u, v$ ) on the tangent plane can be calculated as:

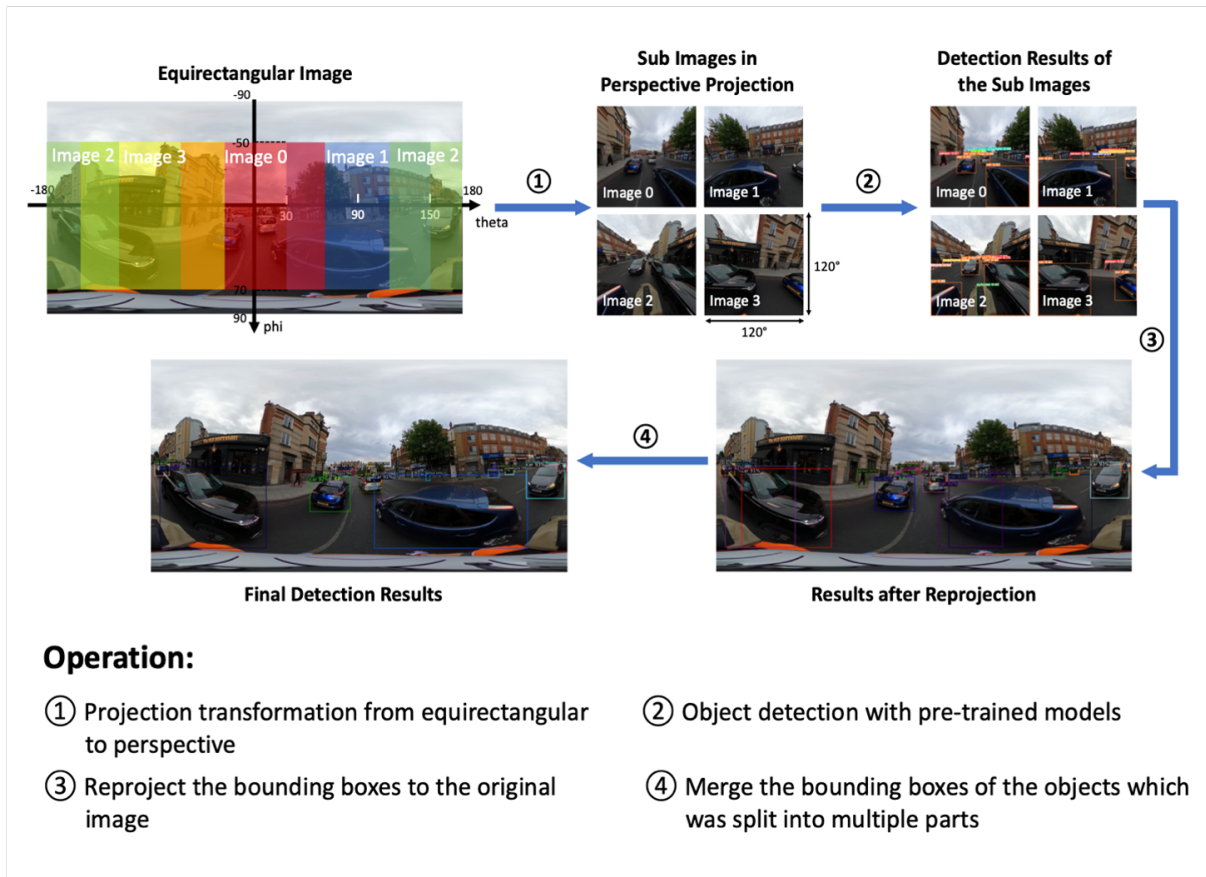


Figure 8: Workflow of the proposed method for improving object detection on panoramic images

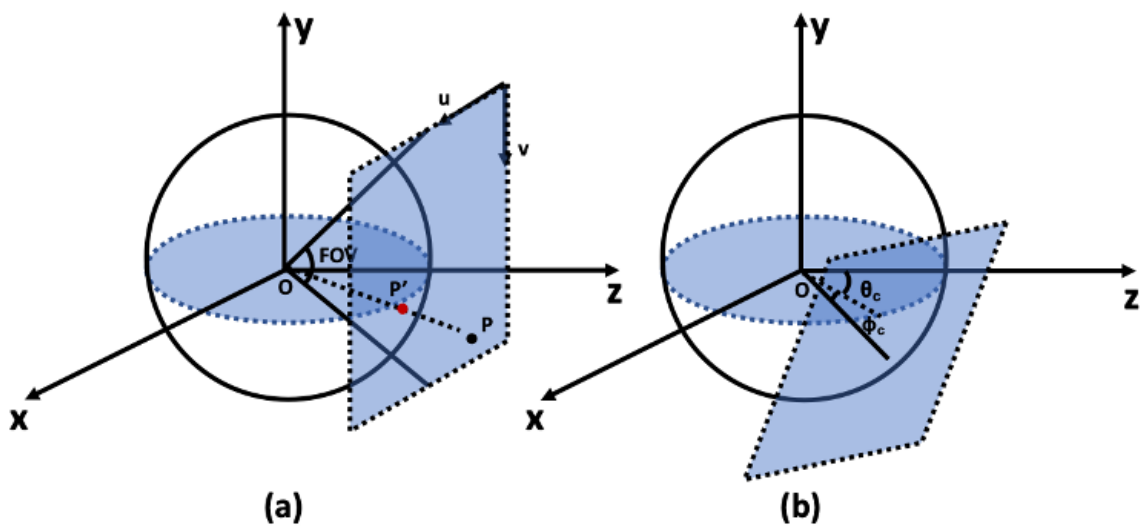


Figure 9: Two cases of projection from a sphere to a plane: (a) towards the z-axis (b) towards any direction

$$X = \frac{u - T}{\sqrt{u^2 + v^2 + 2T^2 - 2uT - 2vT + 1}} \quad (1)$$

$$Y = \frac{-v + T}{\sqrt{u^2 + v^2 + 2T^2 - 2uT - 2vT + 1}} \quad (2)$$

$$Z = \frac{1}{\sqrt{u^2 + v^2 + 2T^2 - 2uT - 2vT + 1}} \quad (3)$$

Where  $T$  is the tangent of the half of the field of view of the projection, i.e.,  $T = \tan(\frac{FOV}{2})$ .

If represented in a geographic coordinate system, P' can be also represented as longitude  $\phi$  and latitude  $\theta$  (Lee & Han, 2021):

$$\phi = \tan^{-1}\left(-\frac{Z}{X}\right) \quad (4)$$

$$\theta = \sin^{-1}\left(\frac{Y}{\sqrt{X^2 + Y^2 + Z^2}}\right) \quad (5)$$

As Figure 9 (b) shows, if the projection is not towards the z-axis, when calculating the coordinates of point P' ( $X', Y', Z'$ ), a rotation equation  $R$  should be applied as follows (Lee & Han, 2021):

$$\begin{bmatrix} X' \\ Y' \\ Z' \end{bmatrix} = R \begin{bmatrix} X \\ Y \\ Z \end{bmatrix} = \begin{bmatrix} \cos\alpha & -\sin\alpha\sin\theta_c & \sin\alpha\cos\theta_c \\ 0 & \cos\theta_c & \sin\theta_c \\ -\sin\alpha & -\sin\theta_c\cos\alpha & \cos\alpha\cos\theta_c \end{bmatrix} \begin{bmatrix} X \\ Y \\ Z \end{bmatrix} \quad (6)$$

Where  $\alpha = \phi_c + \frac{\pi}{2}$ ,  $\phi_c$  is the angle between the projection direction and plane  $xoz$ , while  $\theta_c$  is the angle between the projection direction and plane  $yoze$ .

In this project, the `GetEquirec()` function of the `Perspective-and-Equirectangular` library in Python (timt90022, 2018) was called to realise this projection transformation. It provides FOV, theta and phi parameters, which correspond to  $FOV$ ,  $\theta_c$  and  $\phi_c$  in Equations (1) to (6).

To identify these parameters, this research referred to the position distribution analysed in subsection 3.3.1: since almost all the objects in the videos are distributed from  $-50^\circ$  to  $70^\circ$  vertically, FOV and phi were set to  $120^\circ$  and  $-10^\circ$ , so that only the objects within this interval would be projected and detected in the improved models.

Although three sub-images with a  $120^\circ$  FOV are enough to cover an equirectangular image horizontally, because there are still some distortions in the perspective images, objects near the edges of the sub-images may not be detected. To solve this problem, this paper chose to project the original image into 4 sub-windows along the lines of  $0^\circ$ ,  $90^\circ$ ,  $-180^\circ$  and  $-90^\circ$  longitude (i.e., theta) — since there is an overlap of  $30^\circ$  between each pair of adjacent sub-images, objects within  $15^\circ$  from an edge in one sub-image, such as the circled person in Figure 10, must be shown closer to the centre in another sub-image,



Figure 10: Projections of an object in different sub-images: The closer it is to the edges of a sub-image, the greater distortions it may have

which results in less severe distortions.

346

#### 4.1.2 Object Detection with Pre-trained Models

347

Although any model can be used to predict bounding boxes for the sub-images, in order to check whether the proposed method can improve the performance of different types of pre-trained models, this paper chose YOLO v5 and Faster RCNN, the representatives of one-stage and two-stage models, to perform object detection.

348

349

350

351

Both Faster RCNN and YOLO v5 provide several models with different structures, which are designed for different speed and accuracy requirements. In this step, Faster RCNN-FPN (ppwwyyxx, 2021) and YOLOv5m6 (Ultralytics, 2020) pre-trained on the COCO dataset were chosen for they are moderate in both speed and accuracy.

352

353

354

355

By default, the bounding boxes predicted by Faster RCNN are output in the following format:  $(X_{min}, Y_{min}, X_{max}, Y_{max})$ , where  $(X_{min}, Y_{min})$  and  $(X_{max}, Y_{max})$  are the coordinates of the top-left and bottom-right corners of a box, while YOLO outputs the boxes in  $(X, Y, W, H)$  format, where  $(X, Y)$  are the coordinates of the centre point, and  $W, H$  represent the width and height of a box. Thus, to unify the formats, detection implemented by YOLO was converted with the following equations:

356

357

358

359

360

361

$$X_{min} = X - W/2 \quad (7)$$

$$X_{max} = X + W/2 \quad (8)$$

$$Y_{min} = Y - H/2 \quad (9)$$

$$Y_{max} = Y + H/2 \quad (10)$$

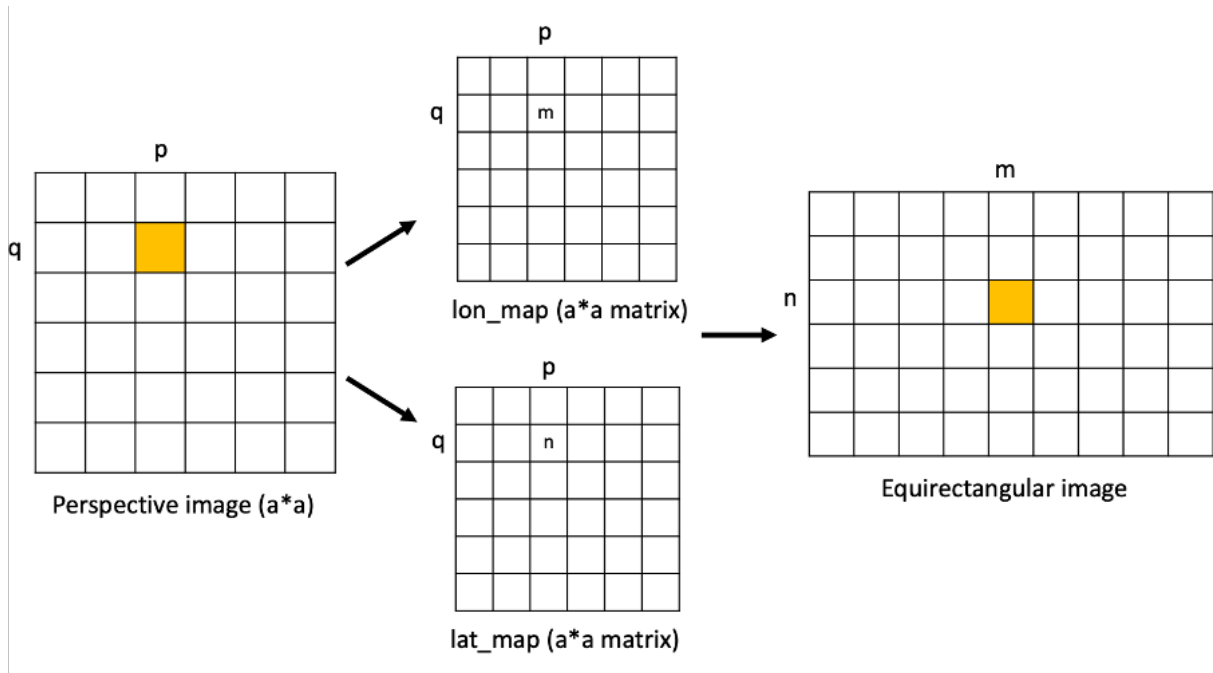


Figure 11: Process of reprojecting a point from perspective to equirectangular

### 4.1.3 Reprojection of the Detection

362

When doing the projection transformation, the `GetEquirec()` function in the `Perspective-363`  
`-and-Equirectangular` library creates two matrices called ‘`lon_map`’ and ‘`lat_map`’ 364  
(timt90022, 2018), which determine where to locate the pixels in the perspective images. 365  
Based on this process, the coordinates of the corresponding point on the equirectangular 366  
image of a point  $(p, q)$  on a perspective sub-image can be represented as  $(m, n)$ , where 367  
 $m$  and  $n$  are the values of  $lon\_map(p, q)$  and  $lat\_map(p, q)$ , respectively, as shown in 368  
Figure 11. 369

As Figure 12 shows, to map all the bounding boxes which are at least  $15^\circ$  away from 370  
the edges back to the original image, every point on the borders of these boxes was 371  
reprojected with the approach above. However, since this process bends the borders, 372  
which makes it hard to output and evaluate the predictions, this project used minimum 373  
bounding rectangles to represent the boxes. 374

Due to the boundary continuity, the detection crossing the centre lines of the sub- 375  
images projected along  $180^\circ$  (i.e., Image 2 in Figure 10) are shown twice near the left 376  
and the right edges respectively in equirectangular views. Thus, when dealing with such 377  
detection, as illustrated in Figure 13, instead of directly projecting the whole box, this 378  
study first divided each of them into two parts along the centre line, and then projected 379  
them separately, so that the detection outputs can be displayed and evaluated correctly. 380

### 4.1.4 Merging the Reprojected Bounding Boxes

381

As the final step of the proposed workflow, for merging the bounding boxes of the objects 382  
that cannot be fully displayed in a single sub-image, the boxes with at least one side 383

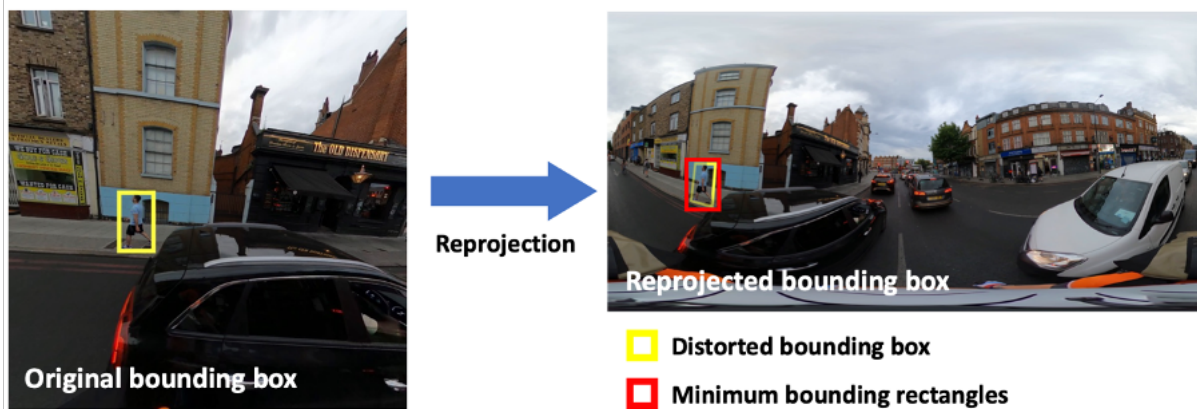


Figure 12: Process of reprojecting a bounding box from perspective to equirectangular

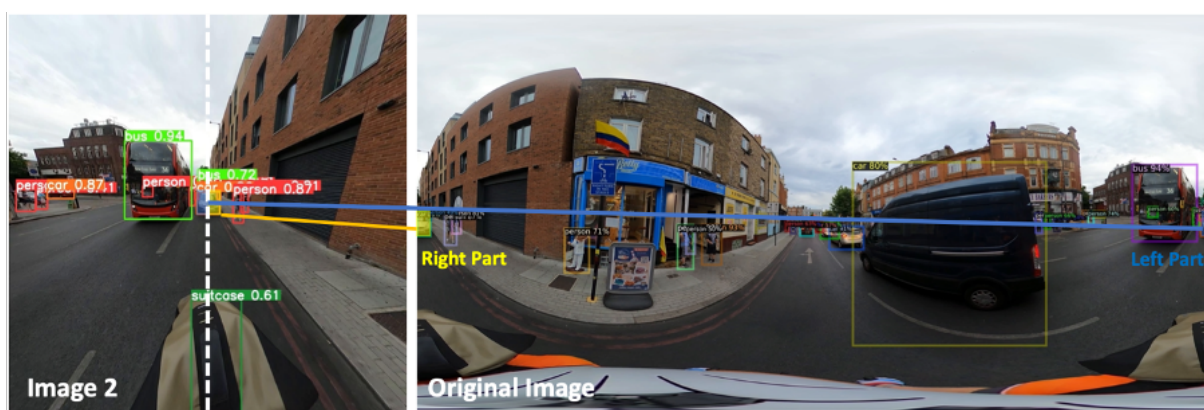


Figure 13: Process of reprojecting an object which is across the boundaries



Figure 14: Method for processing the objects which are displayed in several sub-images

coinciding with a boundary of a sub-image were picked out. According to Figure 14, first, such boxes that are entirely within the 30-degree-wide overlapped areas were removed, as they must be included in another bounding box with smaller distortions. Then, for the boxes of the same category which are tangent to consecutive boundaries, the project combined them into their MBRs, while the score of each new bounding box was calculated as the area-weighted average.

#### 4.1.5 Model Evaluation

For the evaluation of the improving effect of the proposed method, after designing and implementing each step of the workflow, using the methods in the `COCOEvaluator` class of `Detectron2` (ppwwyyxx, 2021), this paper tested the pre-trained Faster RCNN-FPN and YOLO v5m6 before and after the method was applied on the dataset built in Chapter 3 under different input resolution settings (640, 1280, 1920). These models' mean average precision (mAPs) metrics and average precision (APs) metrics of different sizes were recorded and compared, as higher APs indicate better object detection performance.

In addition, to prove the effect of merging the bounding boxes, which is an innovation compared to the method in Yang et al. (2018)'s study, this project also compared the models with and without combining the bounding boxes in the same way.



garian algorithm is used again to do the data association. After that, for each unmatched 422  
detection, DeepSORT creates new tracks for them, treating them as objects new to the 423  
video; while for the unmatched tracks, if they are ‘unconfirmed’ or have not been matched 424  
for more than a certain number of frames, DeepSORT removes them from the track list. 425

#### 4.2.2 Applying the Improved Object Detection Models 426

For testing on the data that are annotated in COCO format, the object detection models 427  
improved in subsection 4.1 output the predictions in the following format:  $(X_{min}, Y_{min},$  428  
 $X_{max}, Y_{max})$ . Since DeepSORT only supports inputs in  $(X, Y, W, H)$  format, before being 429  
input into DeepSORT, each prediction from the detector was converted with the following 430  
equations: 431

$$X = (X_{min} + X_{max})/2 \quad (11)$$

$$Y = (Y_{min} + Y_{max})/2 \quad (12)$$

$$W = X_{max} - X_{min} \quad (13)$$

$$H = Y_{max} - Y_{min} \quad (14)$$

Where  $X_{min}, X_{max}, Y_{min}, Y_{max}, W, H$  have the same definition as previously. 432

#### 4.2.3 Introducing the Support for Category Information 433

As mentioned above, when associating the detections with tracks using cosine, Mahalan- 434  
obis and IOU distances, DeepSORT ignores the category information of the detection, 435  
treating objects of different categories equally. Thus, tracks and detections can be wrongly 436  
matched when their corresponding values in the cost matrices are small. In fact, if apply- 437  
ing the original model to panoramic cycling videos, such wrong associations can be seen 438  
when objects of different categories alternate at a short distance. As shown in Figure 439  
16, since the bike in the right image appears not far away from where person 89 left the 440  
video, the track representing the person is wrongly matched with the bike. 441

In response to the problem, a new attribute called ‘\_class’ was added to the Track class 442  
of DeepSORT. Detection categories were also input into DeepSORT. In that way, when 443  
a track is initiated, its ‘\_class’ attribute will be set as the category of the corresponding 444  
detection. 445

In addition, whenever the cost matrices were formed, as shown in Figure 17, category 446  
filtering was performed to set all the values representing the distances between objects 447  
and detections of different classes to  $10^5$ , so that the existing tracks can only get matched 448  
with the detections of the same categories. 449

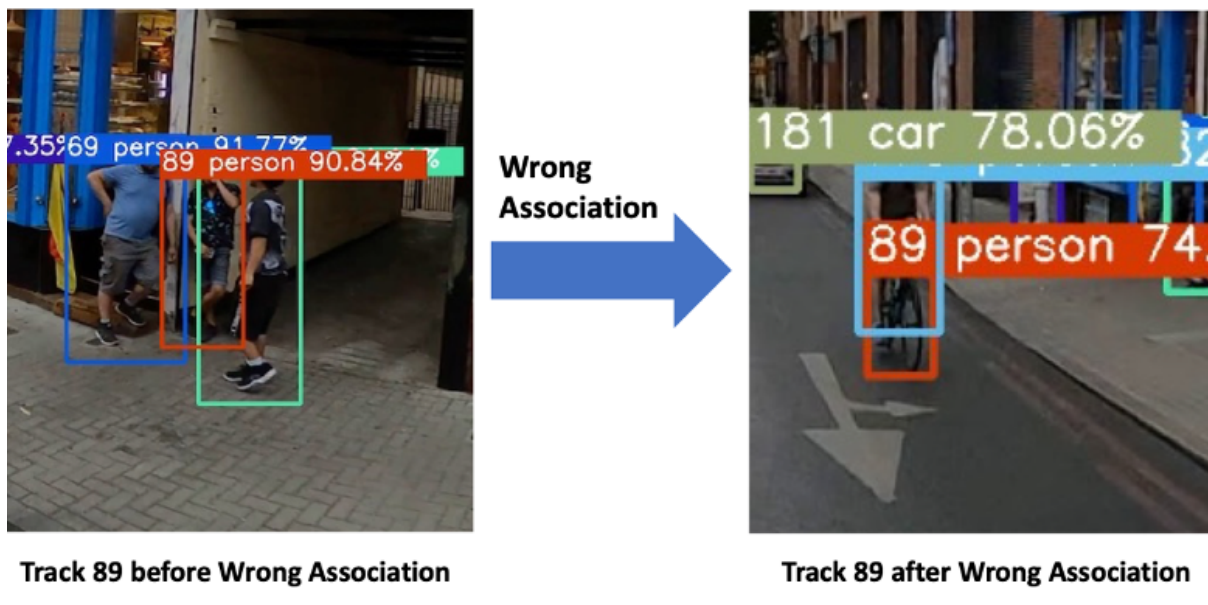


Figure 16: An example of wrong associations between tracks and detections

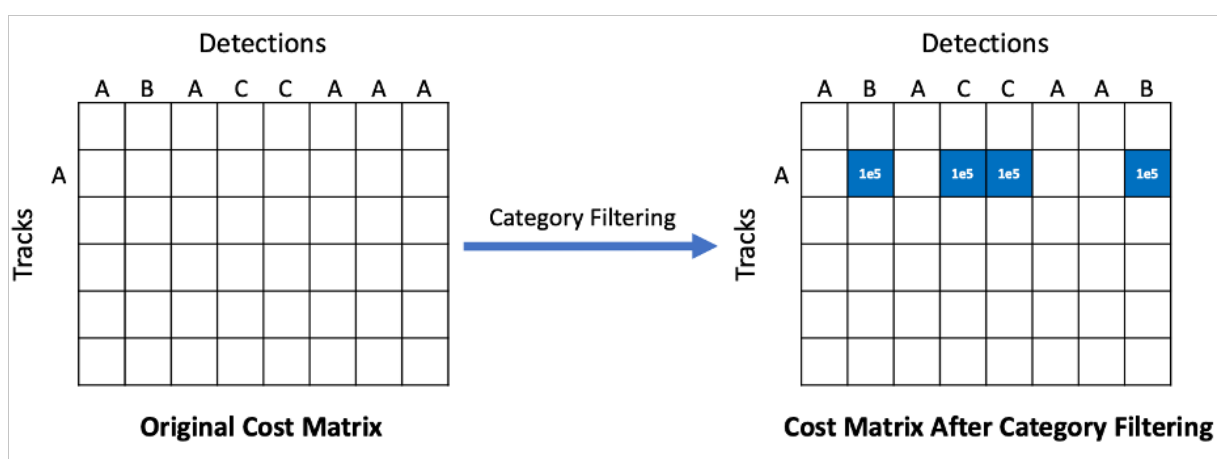


Figure 17: Process of category filtering on a cost matrix



Figure 18: Method for tracking the detections which are shown twice in one frame

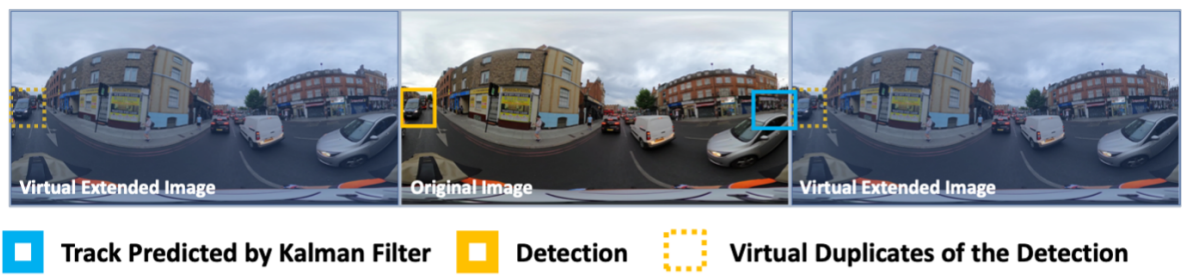


Figure 19: Preparations for the improved distance calculation process (suitable for Mahalanobis distance and IOU distance)

#### 4.2.4 Introducing the Support for Boundary Continuity

450

To track the detections which are divided into two parts (i.e., objects crossing the centre 451  
 lines of the sub-images projected along  $180^\circ$ ), this research proposes an approach referring 452  
 to the annotation method for panoramic MOT designed in subsection 3.2: As shown in 453  
 Figure 18, the first step is to move each of the left bounding boxes to the right and merge 454  
 it with the right box; Then, input the combined bounding boxes into DeepSORT directly, 455  
 despite the fact they are beyond the boundaries. 456

In addition, to avoid ID switching caused by objects that leave from one side of the 457  
 image and return from the other side, the distance calculation process of DeepSORT was 458  
 also improved. As Figure 18 shows, for calculating the Mahalanobis or IOU distance 459  
 between a predicted track and a detection, the proposed method first duplicates the 460  
 detection twice on two virtual images extended from both sides of the original image; 461  
 Then, it calculates the distances from the track to these three bounding boxes respectively 462  
 and selects the shortest one to fill the cost matrix. 463

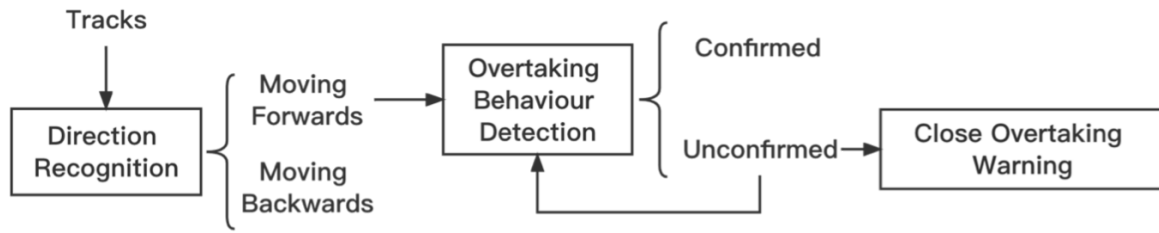


Figure 20: Workflow of the application which can detect the overtaking behaviour of the surrounding vehicles

#### 4.2.5 Model Evaluation 464

To evaluate the proposed method for improving MOT on panoramic cycling videos, the research used DeepSORT before and after an improved detection model was applied, and also before and after the support for category information and boundary continuity were introduced, to track the objects of interest in the 3 annotated videos. Then, by comparing their results with the ground truth using `py-motmetrics` (cheind, 2019), the project also calculated the evaluation metrics of the models, which can be used to analyse and compare the MOT performance of different models.

In addition, for qualitative analysis of the tracking effects, the results were also exported as videos marked with bounding boxes, track ids, categories and confidence scores.

### 4.3 Automated Overtaking Behaviour Detection 474

In the last step of the proposed methodology, an application was designed and developed, which can use the tracking results to detect the overtaking behaviour of the vehicles. As shown in Figure 20, for each image frame, the application first classifies each vehicle into ‘forwards’ or ‘backwards’ according to the movement of its track; After that, overtaking behaviour is detected among the vehicles moving forwards, and the detected overtakes are divided into two states: confirmed (completed) and unconfirmed (ongoing) — For the confirmed overtakes, the application outputs their start and end frames with the track IDs; while for the unconfirmed ones, if they are close to the camera, the application can warn the users of their current directions, so that the cyclists can react to the potential dangers in advance. It should be noted that overtaking is used as a test case to demonstrate the model and different actions can be detected by changing the type, direction and location (left or right of the rider) of the tracked objects.

In the following subsections, each module of the application is described in detail and an experiment is carried out to evaluate the detection accuracy of the application.

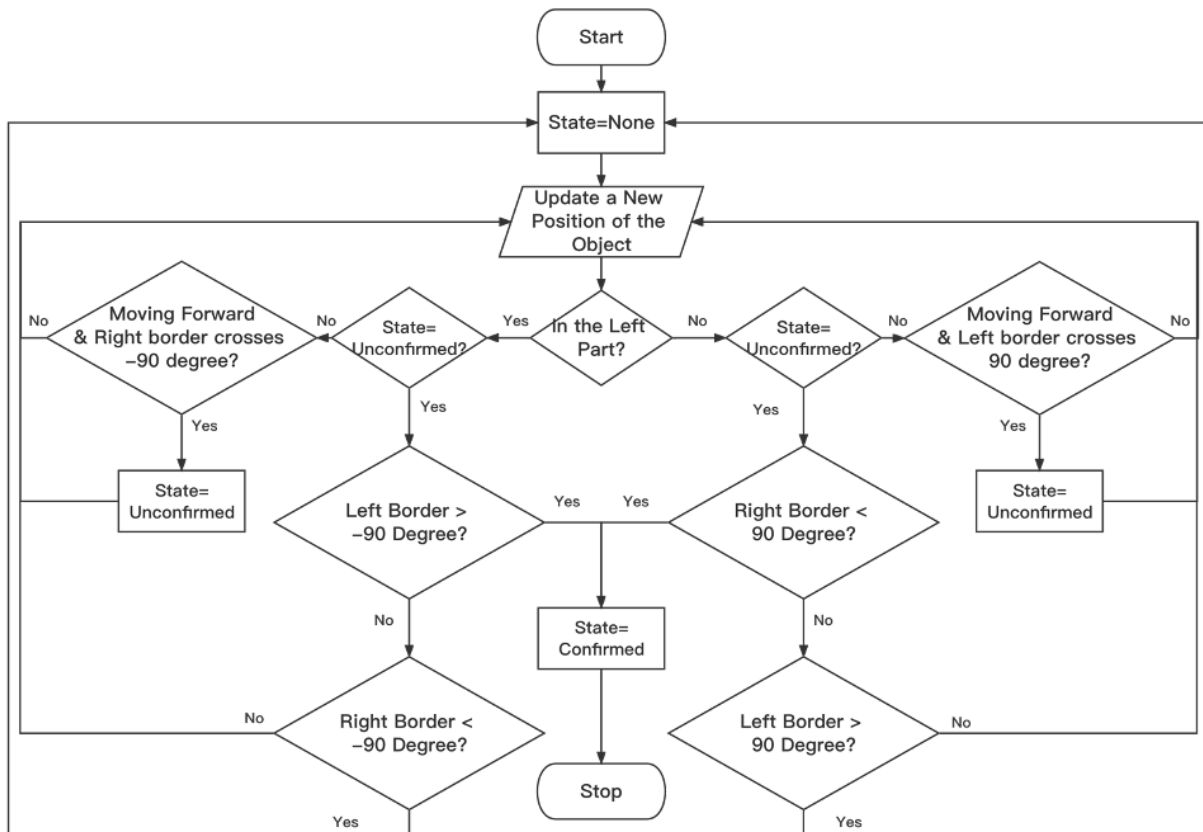


Figure 21: Flow chart of the overtaking behaviour detection for a specific object

### 4.3.1 Movement Direction Recognition

489

According to the definition of equirectangular projection (Snyder, 1997), in a panoramic video, objects behind the camera are shown on the left and right sides, while objects in the front are shown in the middle. Therefore, if an object's current position is closer to the centre line compared to its position in the last frame, it is moving forwards relative to the camera. Similarly, if an object moves away from the centre, it is moving backwards.

However, in practice, judging the moving directions based on only two frames is not rigorous: In some frames where the camera moves slightly with the rotation of the cyclists' head, some objects may incorrectly move in the opposite direction. Thus, to judge the movement of an object, this project calculated its movement in each of the last 5 frames relative to the previous frame. If more than 3 of them were forward, then it was classified as 'forwards'. Likewise, if more than 3 of the movements were backwards, then the object was classified as 'backwards'.

### 4.3.2 Overtaking Behaviour Detection

502

The project defined overtaking behaviour as the act of a motor vehicle moving forwards and completely passing the cyclist. In an equirectangular video, this definition can be abstracted as the occasion in which the front and rear of a vehicle on the left (or right) side of the image cross the  $-90^\circ$  (or  $90^\circ$ ) longitude line in order.

Figure 21 shows how the application was designed to realise the overtaking behaviour 507  
detection on a specific object in the panoramic videos: Take a vehicle on the left side of 508  
the video as an example, if the right side of its bounding box crosses the  $-90^\circ$  longitude 509  
line for the first time as it is moving forwards, it will be assigned with an unconfirmed 510  
(ongoing) overtake. The overtake will remain unconfirmed until the left boundary of the 511  
bounding box passes the  $-90^\circ$  line or the right border goes back to the left of the line, 512  
which means the overtake is finished (confirmed), and the overtake is failed, respectively. 513

### 4.3.3 Application Evaluation 514

To evaluate how well the application can detect the overtaking behaviour of the vehicles, 515  
this project used the application to perform detections on Video 4, 5 and 6 trimmed in 516  
Section 3. After all the detections had finished, the corresponding bounding boxes in the 517  
period of each overtake were marked in red. Then, according to these marked objects, this 518  
project manually counted the number of TP (correctly detected overtakes), FP (wrong 519  
detections) and FN (undetected overtakes) and calculated the precision and recall using 520  
Formula 1 and 2. In addition, to explore how the improved MOT and object detection can 521  
affect the performance of overtaking detection, the project also compared the applications 522  
using models without the proposed modifications. 523

## 5. Results & Analysis 524

After implementing the proposed methodology, in this chapter, the project will present 525  
and analyse the results obtained in each step systematically. 526

### 5.1 Evaluation of the Model for Improving Object Detection on 527 Panoramic Cycling Images 528

The experiments designed in subsection 4.1.5 were implemented on a server equipped 529  
with an NVIDIA Tesla P100 GPU and an Intel Xeon E5-2630 processor, whose results 530  
are shown in 4. 531

As the baseline models, the original pre-trained Faster RCNN-FPN and YOLO v5m6 532  
are first compared. From Table 4, it can be seen that: the average precision of both models 533  
increase with the growth of input resolution, and according to their APs, APm and API, 534  
this increase is mainly due to the better prediction performance on objects smaller than 535  
 $128^2$ ; In addition, although YOLO v5m6 is a one-stage model, since it is newly released, 536  
under the same input resolution settings, it can always achieve an accuracy similar to, or 537  
even better than that of Faster RCNN at twice the speed. 538

Then, the modified models are compared with the original ones. According to Table 4, 539  
thanks to the smaller distortions of perspective projection, under the same input resolution 540  
settings, the proposed method can significantly improve the detection performance for 541

Pre-Trained Model	Input size	Model	AP	APs**	APm**	API**	FPS
Faster RCNN-FPN	640	Original	8.098	2.342	19.343	<b>40.450</b>	<b>1.52</b>
		Proposed (No Merging)	15.209	10.097	31.639	34.194	0.76
		Proposed (Merging)	<b>16.019</b>	<b>10.097</b>	<b>31.640</b>	38.823	0.83
	1280	Original	17.332	10.497	34.224	<b>47.976</b>	<b>1.46</b>
		Proposed (No Merging)	20.303	15.771	35.439	34.608	0.43
		Proposed (Merging)	<b>20.990</b>	<b>15.772</b>	<b>35.490</b>	38.397	0.42
	1920	Original	20.586	14.431	35.546	<b>45.880</b>	<b>1.40</b>
		Proposed (No Merging)	20.326	15.830	35.634	34.446	0.25
		Proposed (Merging)	<b>21.046</b>	<b>15.830</b>	<b>35.694</b>	38.345	0.24
YOLO v5m6	640	Original	8.271	1.808	19.761	<b>47.092</b>	<b>3.60</b>
		Proposed (No Merging)	15.108	10.210	33.975	32.804	0.86
		Proposed (Merging)	<b>16.107</b>	<b>10.210</b>	<b>34.062</b>	38.292	0.85
	1280	Original	16.910	9.588	34.943	<b>49.679</b>	<b>3.37</b>
		Proposed (No Merging)	24.442	20.789	37.419	35.875	0.46
		Proposed (Merging)	<b>25.428</b>	<b>20.789</b>	<b>37.462</b>	39.456	0.45
	1920	Original	23.211	16.861	37.705	<b>49.184</b>	<b>3.02</b>
		Proposed (No Merging)	29.265	26.171	40.000	32.590	0.26
		Proposed (Merging)	<b>30.144</b>	<b>26.171</b>	<b>40.050</b>	36.326	0.25

Table 4: Average Precision Metrics of Faster RCNN-FPN and YOLO v5m6 before and after the Proposed Methods are Applied

Bolded values represent the best results

\*\* APs, APm and API are the average precision metrics of the small  $(0, 128^2)$ , medium  $[128^2, 384^2)$ , and large  $[384^2, +\infty)$  objects.

small  $(0, 128^2)$  and medium  $[128^2, 384^2)$  objects of both models. However, since multiple projections split some long objects into several parts, before applying the operation of merging the bounding boxes, the proposed models' precision metrics for large objects are much lower than those of the original models.

Merging the bounding boxes can effectively mitigate this problem because, from the table, it is obvious that no matter what the input resolution is, it can always raise the API by at least 3. But, the improved precision for large objects are still slightly smaller than those of the original models.

Nevertheless, since as Figure 6 shows, more than 90% of the objects in the collected videos are small or medium ones, in most cases, no matter whether merging the boxes or not, the mean APs of the proposed models exceed those of the original models by 5, which are even close to the results of the original models under higher input resolution settings.

In terms of inference speed, due to the requirement for sequential detection on 4 sub-images, the improved models are slower than the original ones. However, since even the speeds of the original models are far from real-time detection (30 FPS), this project considers this decrease in speed acceptable.

Model	IDF1	GT	MT	PT	ML	FP	FN	MOTA
Original YOLO + Original DeepSORT	57.0%	218	34	<b>100</b>	84	<b>1513</b>	11479	45.3%
Improved YOLO + Original DeepSORT	<b>65.3%</b>	218	<b>131</b>	63	<b>24</b>	7246	<b>4892</b>	<b>48.7%</b>

Table 5: Evaluation Metrics of Original DeepSORT before and after an Improved Detection Model (YOLO v5m6, Input Size: 1280) is Applied. Best results in bold

Model	IDF1	FP	FN	IDs	FM	MOTA	MOTP	Time (s)
Improved YOLO + Original DeepSORT	65.3%	7246	4892	181	<b>392</b>	48.7%	0.231	<b>0.056</b>
Improved YOLO + DeepSORT (Category Support)	64.7%	7235	4878	185	394	49.8%	0.231	<b>0.061</b>
Improved YOLO + DeepSORT (Category and Boundary Support)	<b>66.7%</b>	<b>6344</b>	<b>4795</b>	<b>179</b>	<b>392</b>	<b>52.9%</b>	0.231	0.066

Table 6: Evaluation Metrics of DeepSORT before and after the Supports for Category Information and Boundary Continuity are Introduced. Best results in bold

## 5.2 Evaluation of the Model for Improving Multiple Object Tracking on Panoramic Cycling Videos

The experiments designed in subsection 4.2.5 were implemented on the same server. Since according to Table 4, YOLO v5m6 gets a high accuracy at a moderate speed when the input size is 1280, it was used as the detector of DeepSORT in these experiments.

First, DeepSORT models before and after the improved YOLO is applied are compared, whose results are shown in Table 5. Since comparing some metrics such as ID switch is meaningless when the detectors are different, only IDF1, MT, PT, ML, FP, FN and MOTA are compared here.

From the Table, it can be seen that the improved detector significantly reduces the number of false negatives. As a result, according to the values of MT (Mostly Tracked), PT (Partially Tracked) and ML (Mostly Lost), much more ground truths are successfully tracked. In addition, the proposed detector also raises IDF1 by 8.3%, which shows the model using the improved YOLO can track objects more continuously. Although the proposed detector also increases the number of FP, in terms of MOTA, it effectively improves the MOT performance of DeepSORT.

Then, using the improved YOLO as detectors, models before and after the implementations of supports for category information and boundary continuity are compared, whose results are shown in Table 6.

From the table, the support for category information reduces FP and FN. As a result, MOTA rises from 48.7% to 49.8%. Although the improving effect on metrics seems relatively slight,

### Example 1



### Example 2



### Example 3

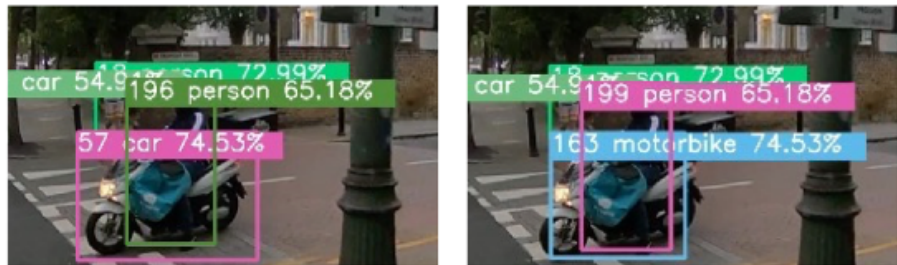


Figure 22: Examples of how category information avoids incorrect data matching (Left: Original DeepSORT; Right: DeepSORT with Support for Category Information)

through observing the output videos of the models with and without the support for category information, it can be seen that some incorrect data matching has been successfully avoided, as shown in Figure 22.

On the basis of the introduction of category information, support for boundary continuity further enhances the accuracy of data association, for it increases MOTA by 3%. In addition, according to the higher IDF1 score and the fewer ID switches, it can be seen that the tracking continuity of DeepSORT on panoramic cycling videos is enhanced.

These enhancements are also evident in the output tracking videos: With the support for boundary continuity, DeepSORT can now treat the two parts of the same object (such as car 3 in Figure 23) as a whole; In addition, using the improved distance calculation method, DeepSORT is now capable of keeping the ids of the objects (such as human 11 in Figure 24) that leave from one side of the image and return from the other side.

In terms of tracking speed, for each image frame, support for category information and boundary continuity only take DeepSORT 0.01 seconds longer to finish the data association. Considering the significant performance improvements provided by the proposed method, such a small drop in speed acceptable.



Figure 23: Tracking results of the objects which are shown in two parts before and after the support for boundary continuity is introduced

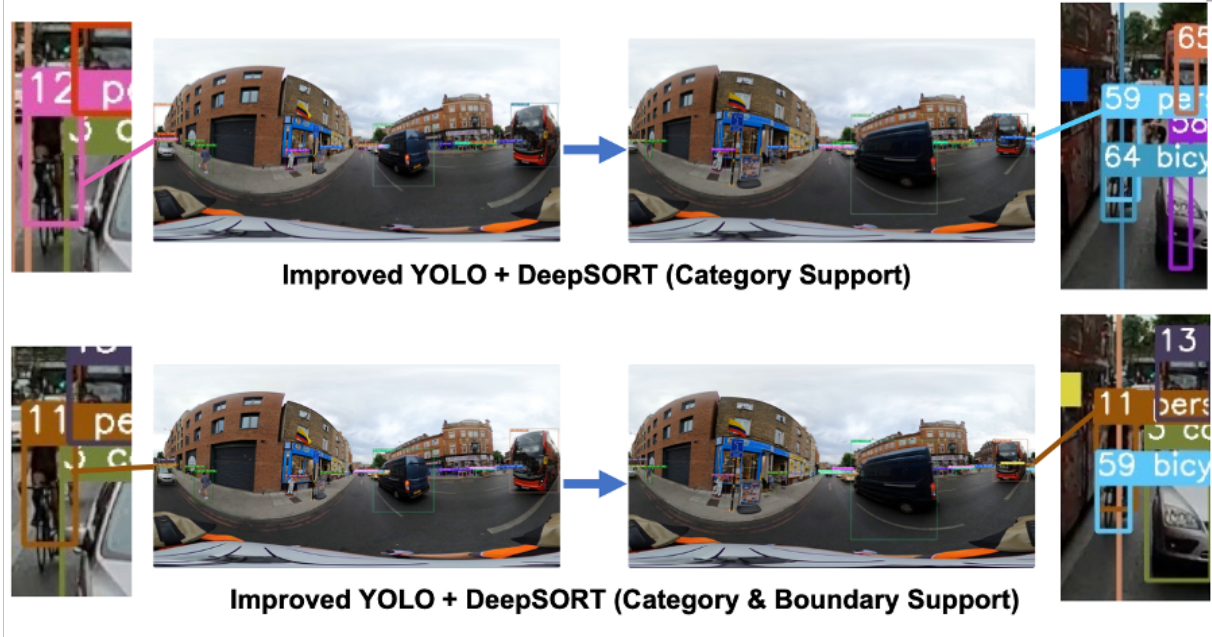


Figure 24: Tracking results of the objects which leave from one side of the image and return from the other side before and after the support for boundary continuity is introduced

Model	TP	FP	FN	Recall	Precision	FPS
Original YOLO v5m6 + Original DeepSORT	53	0	1	98.15%	100%	2.75
Improved YOLO v5m6 + Improved DeepSORT	54	0	0	100%	100%	0.43

Table 7: Evaluation Results of Overtaking Behaviour Detection - Experiment 1

### 5.3 Evaluation of the Automated Overtaking Behaviour Detection

To evaluate the performance of overtaking behaviour detection, two validation tests are carried out. The first test compares the performance of the proposed model against the Original YOLO v5m6 + Original DeepSORT to assess the relative performance of each model. The second test applies the proposed model to a range of videos collected under different riding conditions in London, UK.

In the first experiment, under the input resolution setting of 1280, two combinations of models were tried: the Original YOLO v5m6 + Original DeepSORT, and the Improved YOLO v5m6 + Improved DeepSORT. Their evaluation results are shown in Table 7.

When being used for automated overtaking behaviour detection, the application using the tracking results of the original models correctly detects 53 of 54 overtakes recorded in Video 3, 4 and 5, while on the basis of that, the one using the improved models successfully identifies the missed overtake, thus obtains a recall and precision of 100%.

By observing the only difference between the results of the two applications, as shown in Figure 25, it can be seen that in the application using the original models, since there is no support for multiple categories, the vehicle is incorrectly matched with a traffic light, thus its movement is ignored. As a comparison, the proposed models effectively eliminate wrong associations, which results in the successful detection of the overtaking behaviour of this vehicle.

Although the proposed models bring higher detection accuracy, due to the lower inference speed of the proposed object detection model, the overall FPS of the application using the improved models is 2.3 frames slower than that using the original models.

	Predicted Positive	Predicted Negative
Actual Positive	44	6
Actual Negative	6	44

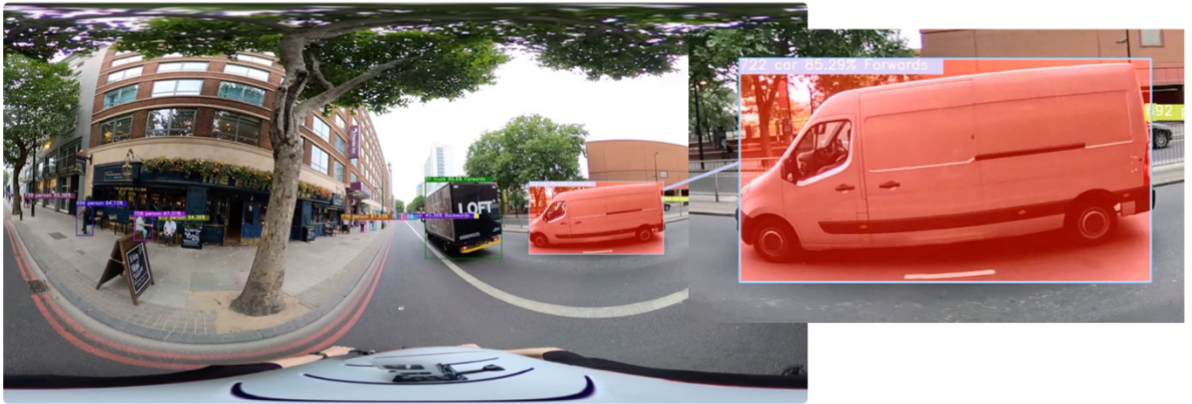
Table 8: Evaluation Results of Overtaking Behaviour Detection - Experiment 2

In the second experiment, we tested the improved algorithm on one hundred 15-second 360° video clips filmed by 49 different cyclists, who were participants in UCL’s 100 Cyclists Project. The participants used the GoPro Max camera to record their activities over a period of two weeks, and were instructed to say ‘near-miss’ when experiencing a near-miss event. The test results are presented as a confusion matrix in Table 8.

It can be seen that the algorithm demonstrates both specificity and sensitivity of  $44 \div 50 = 0.88$ , and the F-score of  $(2 \times 44) \div (2 \times 44 + 6 + 6) = 0.88$ . All 6 videos classed as positive by the algorithm that do not contain overtaking have very quick ‘flash’ classifications lasting one or several frames and are due to the



**Original YOLO + Original DeepSORT**



**Improved YOLO + Improved DeepSORT**

Figure 25: The instance which gets different detection results in different applications



Figure 26: Example of a ghost bus, which in fact is a shop front that is classed as a bus in a single frame, leads to an erroneous overtaking detection

occasional incorrect object detection by YOLO. An example of a bus being erroneously detected, 631 which is in fact a shop front, is depicted in Figure 26. Applying a minimum time threshold for 632 the overtaking manoeuvre, such as 0.5 or 1 seconds, would eliminate all false positives in our 633 training set. To solve this problem during real-time overtaking detection, one could introduce a 634 lag of several frames and only label the behaviour as overtaking after that point. 635

Among the 6 videos classed as false negatives (where overtaking is undetected by the al- 636 gorithm), in 3 videos the overtaking vehicle moves fully or mostly in a lane adjacent to the 637 cyclist, which may or may not be viewed as overtaking. In one exported video, the cyclist’s 638 camera is not properly centred and moves during overtaking. In another video, the cyclist’s food 639 delivery-style backpack, as well as rain drops, partly obstruct the manoeuvre as shown in Figure 640 27. 641

## 6. Discussion 642

### 6.1 Improving Object Detection 643

Although Table 4 indicates that the performance of the proposed method can be also achieved 644 by the original models with larger input resolution, once the input resolution is as large as that 645 of the original image, the effect can not be replaced anymore. In other words, it increases the 646 upper limit of accuracy that an object detection model can achieve on a panoramic image. 647

Conversely, since the prediction performance of the proposed model is always similar to 648 (or even better than) that of the original models with higher input resolution, for the same 649 accuracy requirements, the proposed model consumes fewer GPU resources. Thus, it can achieve 650 competitive accuracy even on low-end GPUs (Yang et al., 2018). 651

Additionally, according to Table 5, the improved object detection models can effectively 652 enhance the performance of MOT models (such as DeepSORT) as more objects can be tracked 653



Figure 27: The cyclist’s food delivery-style backpack, as well as rain drops, partly obstruct the overtaking manoeuvre, preventing the algorithm from detecting the overtaking behaviour

correctly, which is consistent with Bewley et al. (2016) ’s opinion.

654

## 6.2 Improving Multiple Object Tracking

655

First, the proposed method realises the annotation and results output of the objects which go across the boundaries in an equirectangular image without violating the MOT16 annotation rules (Milan et al., 2016). In that way, the existing MOT metrics can be still used for evaluating the tracking results on panoramic videos.

656

657

658

659

What’s more, on the basis of the performance improvement brought by the proposed object detection models, the introduction of category information and support for boundary continuity further enhances the applicability of DeepSORT to panoramic videos by reducing the number of mismatches and ID switches.

660

661

662

663

## 6.3 Overtaking Behaviour Detection

664

The proposed method can detect the completed overtaking behaviour of vehicles in panoramic videos with a high degree of accuracy and can output the start and end frames of each overtake with the corresponding track ID. This precise and automated analysis can provide abundant conflict data for studies on cycling safety in the future.

665

666

667

668

## 6.4 Limitations and Future Work

669

The proposed methodology has some limitations, which will be addressed in future work. Firstly, as multiple projection transformations divide long objects into several parts, according to Table 4, even when bounding box combination has been applied, the proposed models’ performance on large objects (size > 3842 pixels) is inferior that of the original models. As shown in Figure 28, this can be explained by some parts of large objects (such as the blue car in sub-image 1)

670

671

672

673

674

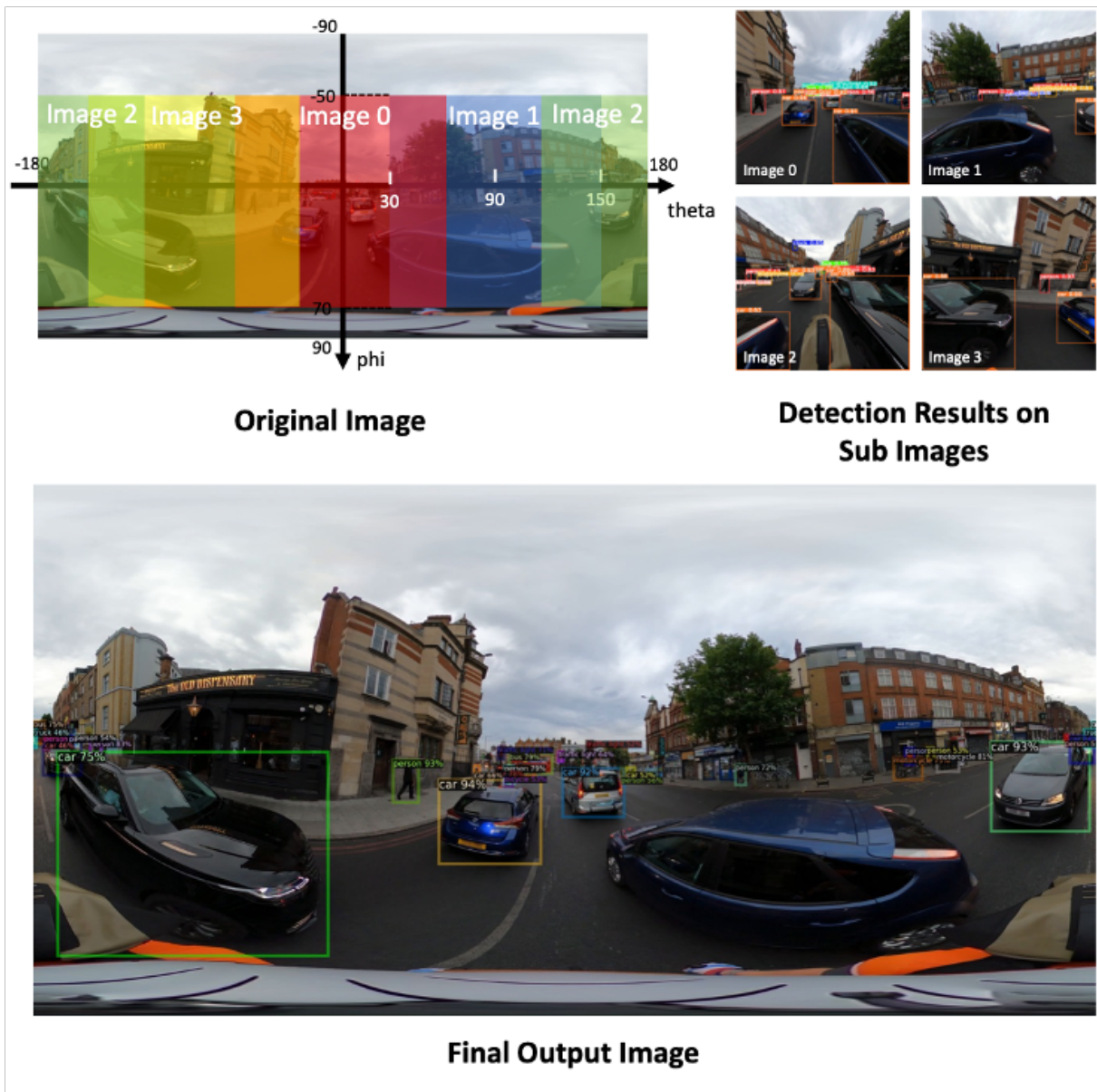


Figure 28: Example of unsuccessful detection of the proposed model on objects across the sub-images

not being detected at all, preventing them from being merged. This issue may be mitigated by increasing the number of sub-images to explore whether more overlapping areas can achieve better detection performance on large objects.

Furthermore, as predictions on sub-images are done sequentially, the inference speed is lower than the original models. This affects the operating speed of MOT and overtaking behaviour detection, which use its results. Multi-processing using, for example, `Torch.Multiprocessing` (PyTorch, 2022) will be used to address this in future work. This will allow inferences on sub-images in parallel.

As an MOT model originally designed for pedestrian tracking, DeepSORT uses the ReID (Re-Identification) network trained on pedestrian datasets (Wojke et al., 2017). Although Zuraimi & Zaman (2021)'s research has demonstrated that it is possible to use DeepSORT to realise MOT on other objects such as vehicles without changing its feature extraction network, the results presented here show that when the angle of a vehicle with respect to the camera changes, some

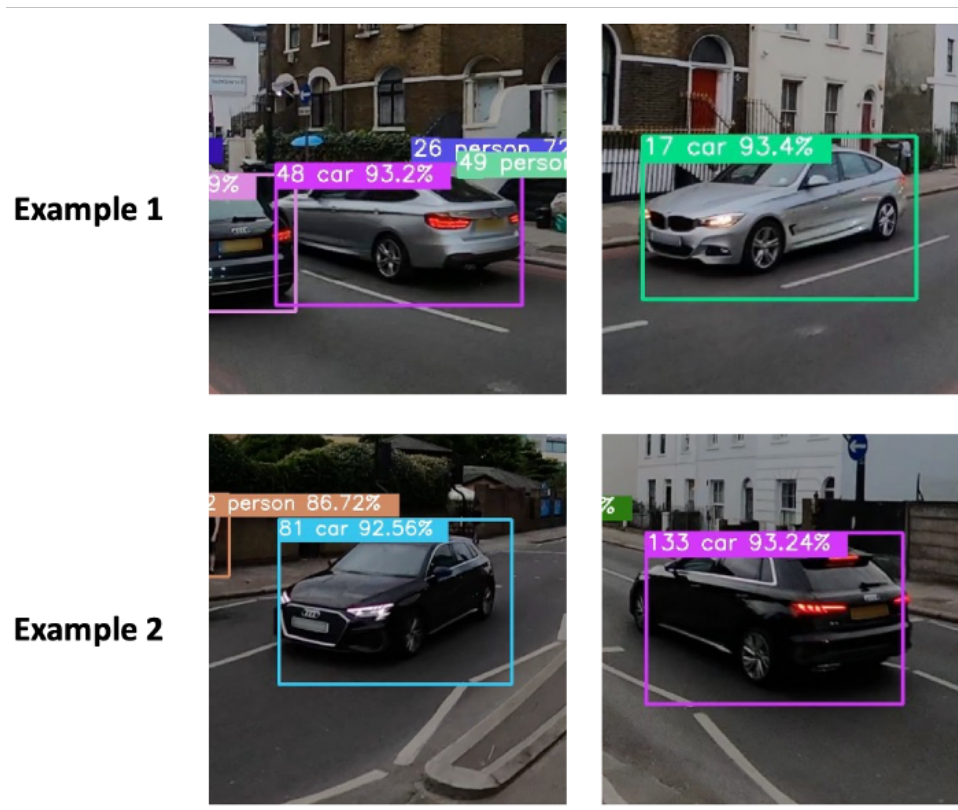


Figure 29: Examples of ID switching when the angle of a vehicle toward the camera changes

ID switching may occur. As Figure 29 shows, using the current ReID network, the matching cascade module in DeepSORT fails in matching the front and rear of these two cars. Referring to Li et al. (2021), this research plans to construct a vehicle image dataset and re-train a ReID network with it, which may improve the performance of DeepSORT in associating the vehicles according to their appearance.

Currently, the moving directions of the vehicles are estimated relative to the cyclists' movement. Since generally, cyclists are unable to move backwards, it is reasonable to use relative forward movements to detect overtakes. However, for the 'backward' objects (those moving from in front of to behind the rider), there are 3 possibilities for their actual movements: moving backwards, being stationary or moving forwards at a slower pace than the cyclist. Thus, if there is no other information such as the speed of the cyclist, other road user behaviours such as braking or reversing may be difficult to detect. Fortunately, the GoPro Max camera, along with many consumer grade action cameras, collects high quality IMU and GPS data, which includes the speed, position, acceleration and orientation of the user. These data will be combined with the video to detect other behaviours associated with cycling risk, such as passing parked vehicles, filtering through traffic or entering the blind spot of heavy goods vehicles (HGVs).

## 7. Conclusion

In the field of cycling safety, most of the existing studies applied computer vision models to 'traditional' videos with a limited field of view for automated road user behaviour analysis (Ibrahim, Haworth, Christie, Cheng & Hailes, 2021). To enable analysis of the complete environment sur-

rounding the rider, this research develops methods for object detection and MOT in panoramic 708  
equirectangular videos. For object detection, existing pre-trained object detection models are 709  
applied to four perspective sub-images projected from equirectangular images. When evaluated 710  
on the annotated panoramic dataset, the AP of YOLO v5m6 and Faster RCNN-FPN are im- 711  
proved under any input resolution setting. For MOT, a method the improved YOLO is used as 712  
the detector and support for boundary continuity and category information is implemented in 713  
DeepSORT, improving MOTA by 7.6% and IDF1 by 9.7%. The tracking results of the improved 714  
DeepSORT are implemented in the case of automated overtaking detection, which achieves high 715  
recall and precision on the testing videos. 716

Although the proposed methodology has been applied to overtaking detection, the framework 717  
is capable of detecting and tracking any objects defined as classes in a pre-trained object detection 718  
model, such as pedestrians, bicycles, buses and motorcycles. Therefore, in future work, methods 719  
will be defined to detect other types of interactions based on the relative motions and positions 720  
of the rider and the objects in their surroundings. 721

If deployed in real-time, these algorithms will enable early warning of potential incidents. 722  
For example, the rider may be alerted to a vehicle preparing to overtake, or may be advised that 723  
they are riding in the ‘car-dooring zone’ next to parked vehicles. Delivery of this information 724  
will necessitate the development of lightweight versions of the algorithms that can be deployed 725  
on edge devices. Given sufficient penetration of action cameras among cyclists, the technology 726  
could be used for crowdsourced risk mapping, whereby risky interactions extracted from video 727  
are mapped to the transport network. These could then be correlated with crash locations from 728  
official data sources to gain a better understanding of overall risk. 729

## References 730

- Ambros, J., Jurewicz, C., Turner, S., & Kieć, M. (2018). An international review of 731  
challenges and opportunities in development and use of crash prediction mod- 732  
els. *European Transport Research Review*, 10(2). [https://doi.org/10.1186/s12544-](https://doi.org/10.1186/s12544-018-0307-7) 733  
[018-0307-7](https://doi.org/10.1186/s12544-018-0307-7) 734
- Avola, D., Cinque, L., Diko, A., Fagioli, A., Foresti, G. L., Mecca, A., Pannone, D., & 735  
Piciarelli, C. (2021). Ms-faster r-cnn: Multi-stream backbone for improved faster 736  
r-cnn object detection and aerial tracking from uav images. *Remote Sensing*, 13(9). 737  
<https://doi.org/10.3390/rs13091670> 738
- Beck, B., Chong, D., Olivier, J., Perkins, M., Tsay, A., Rushford, A., Li, L., Cameron, 739  
P., Fry, R., & Johnson, M. (2019). How much space do drivers provide when 740  
passing cyclists? understanding the impact of motor vehicle and infrastructure 741  
characteristics on passing distance. *Accident Analysis & Prevention*, 128, 253–260. 742  
<https://doi.org/https://doi.org/10.1016/j.aap.2019.03.007> 743
- Bewley, A., Ge, Z., Ott, L., Ramos, F., & Upcroft, B. (2016). Simple online and realtime 744  
tracking. *2016 IEEE International Conference on Image Processing (ICIP)*, 3464– 745  
3468. <https://doi.org/10.1109/ICIP.2016.7533003> 746

- Brunsing, J. (1997). *Public transport and cycling: Experience of modal integration in germany. from the greening of urban transport* (2nd ed.). Wiley (John); Sons, Limited. 747
- cheind. (2019). Py-motmetrics [Accessed 23 August 2022]. [https://github.com/cheind/py-](https://github.com/cheind/py-motmetrics) 748  
[motmetrics](https://github.com/cheind/py-motmetrics) 750
- Daniels, S., Nuyts, E., & Wets, G. (2008). The effects of roundabouts on traffic safety for bicyclists: An observational study. *Accident Analysis & Prevention*, 40(2), 518–526. <https://doi.org/10.1016/j.aap.2007.07.016> 751  
752  
753
- Delmelle, E. M., & Delmelle, E. C. (2012). Exploring spatio-temporal commuting patterns in a university environment. *Transport Policy*, 21, 1–9. [https://doi.org/10.1016/j.](https://doi.org/10.1016/j.tranpol.2011.12.007) 754  
[tranpol.2011.12.007](https://doi.org/10.1016/j.tranpol.2011.12.007) 755  
756
- Deng, F., Zhu, X., & Ren, J. (2017). Object detection on panoramic images based on deep learning. *2017 3rd International Conference on Control, Automation and Robotics (ICCAR)*, 375–380. <https://doi.org/10.1109/ICCAR.2017.7942721> 757  
758  
759
- Fischer, J., Nelson, T., Laberee, K., & Winters, M. (2020). What does crowdsourced data tell us about bicycling injury? a case study in a mid-sized canadian city. *Accident Analysis & Prevention*, 145, 105695. 760  
761  
762
- GoPro. (2021a). Player + reelsteady. [Accessed 25 August 2022]. [https://gopro.com/en/](https://gopro.com/en/us/info/gopro-player) 763  
[us/info/gopro-player](https://gopro.com/en/us/info/gopro-player) 764
- GoPro. (2021b). What is horizon leveling? gopro support. [Accessed 21 August 2022]. <https://community.gopro.com/s/article/what-is-horizon-leveling> 765  
766
- Hels, T., & Orozova-Bekkevold, I. (2007). The effect of roundabout design features on cyclist accident rate. *Accident Analysis & Prevention*, 39(2), 300–307. [https://doi.](https://doi.org/10.1016/j.aap.2006.07.008) 767  
[org/10.1016/j.aap.2006.07.008](https://doi.org/10.1016/j.aap.2006.07.008) 768  
769
- Hua, H., & Ahuja, N. (2001). A high-resolution panoramic camera. *Proceedings of the 2001 IEEE Computer Society Conference on Computer Vision and Pattern Recognition. CVPR 2001*, 1, I–I. <https://doi.org/10.1109/CVPR.2001.990634> 770  
771  
772
- Ibrahim, M. R., Haworth, J., Christie, N., & Cheng, T. (2021). CyclingNet: Detecting cycling near misses from video streams in complex urban scenes with deep learning [eprint: <https://onlinelibrary.wiley.com/doi/pdf/10.1049/itr2.12101>]. *IET Intelligent Transport Systems*, 15(10), 1331–1344. <https://doi.org/10.1049/itr2.12101> 773  
774  
775  
776
- Ibrahim, M. R., Haworth, J., Christie, N., Cheng, T., & Hailes, S. (2021). Cycling near misses: A review of the current methods, challenges and the potential of an ai-embedded system. *Transport Reviews*, 41(3), 304–328. [https://doi.org/10.1080/](https://doi.org/10.1080/01441647.2020.1840456) 777  
[01441647.2020.1840456](https://doi.org/10.1080/01441647.2020.1840456) 778  
779  
780
- Im, S., Ha, H., Rameau, F., Jeon, H.-G., Choe, G., & Kweon, I. S. (2016). All-around depth from small motion with a spherical panoramic camera. In *Lecture notes in computer science* (pp. 156–172). Springer International Publishing. [https://doi.](https://doi.org/10.1007/978-3-319-46487-9_10) 781  
[org/10.1007/978-3-319-46487-9\\_10](https://doi.org/10.1007/978-3-319-46487-9_10) 782  
783  
784
- Jiménez-Bravo, D. M., Lozano Murciego, Á., Sales Mendes, A., Sánchez San Blás, H., & Bajo, J. (2022). Multi-object tracking in traffic environments: A systematic 785  
786

- literature review. *Neurocomputing*, 494, 43–55. <https://doi.org/10.1016/j.neucom.2022.04.087> 787  
788
- Jodoin, J.-P., Bilodeau, G.-A., & Saunier, N. (2014). Urban tracker: Multiple object tracking in urban mixed traffic. *IEEE Winter Conference on Applications of Computer Vision*, 885–892. <https://doi.org/10.1109/WACV.2014.6836010> 789  
790  
791
- Johnson, M., Charlton, J., Oxley, J., & Newstead, S. (2010). Naturalistic cycling study: Identifying risk factors for on-road commuter cyclists [Annual Conference of the Association for the Advancement of Automotive Medicine (AAAM) 2010; Conference date: 01-01-2010]. *Annals of Advances in Automotive Medicine*, 54, 275–283. 792  
793  
794  
795  
796
- LeCun, Y., Bengio, Y., & Hinton, G. (2015). Deep learning. *Nature*, 521(7553), 436–444. <https://doi.org/10.1038/nature14539> 797  
798
- Lee, G.-W., & Han, J.-K. (2021). Viewport rendering algorithm with a curved surface for a wide fov in 360° images. *Applied Sciences*, 11(3), 1133. <https://doi.org/10.3390/app11031133> 799  
800  
801
- Li, J., Liang, X., Wei, Y., Xu, T., Feng, J., & Yan, S. (2017). Perceptual generative adversarial networks for small object detection. *2017 IEEE Conference on Computer Vision and Pattern Recognition (CVPR)*. <https://doi.org/10.1109/cvpr.2017.211> 802  
803  
804
- Li, J., Zang, Z., Xie, H., & Wang, G. (2021). Research on distribution strategy of region of interest in panoramic video based on improved deepsort. *2021 33rd Chinese Control and Decision Conference (CCDC)*. <https://doi.org/10.1109/ccdc52312.2021.9601917> 805  
806  
807  
808
- Lin, T.-Y., Maire, S., Michael an Belongie, Hays, J., Perona, P., Ramanan, D., Dollár, P., & Zitnick, C. L. (2014). Microsoft coco: Common objects in context. In D. Fleet, T. Pajdla, B. Schiele & T. Tuytelaars (Eds.), *Computer vision-eccv 2014* (pp. 740–755). Springer International Publishing. 809  
810  
811  
812
- Liu, K.-C., Shen, Y.-T., & Chen, L.-G. (2018). Simple online and realtime tracking with spherical panoramic camera. *2018 IEEE International Conference on Consumer Electronics (ICCE)*, 1–6. <https://doi.org/10.1109/ICCE.2018.8326132> 813  
814  
815
- Luo, W., Xing, J., Milan, A., Zhang, X., Liu, W., & Kim, T.-K. (2021). Multiple object tracking: A literature review. *Artificial Intelligence*, 293, 103448. <https://doi.org/10.1016/j.artint.2020.103448> 816  
817  
818
- Masalov, A., Ota, J., Corbet, H., Lee, E., & Pelley, A. (2018). Cydet: Improving camera-based cyclist recognition accuracy with known cycling jersey patterns. *2018 IEEE Intelligent Vehicles Symposium (IV)*, 2143–2149. <https://doi.org/10.1109/IVS.2018.8500668> 819  
820  
821  
822
- Massink, R., Zuidgeest, M., Rijnsburger, J., Sarmiento, O. L., & van Maarseveen, M. (2011). The climate value of cycling. *Natural Resources Forum*, 35(2), 100–111. <https://doi.org/https://doi.org/10.1111/j.1477-8947.2011.01345.x> 823  
824  
825

- Milan, A., Leal-Taixe, L., Reid, I., Roth, S., & Schindler, K. (2016). Mot16: A benchmark for multi-object tracking. <https://arxiv.org/abs/1603.00831>
- Mkver. (2014). Ffmpeg [Accessed 18 August 2022]. <https://github.com/FFmpeg/FFmpeg>
- Ojala, R., Vepsalainen, J., & Tammi, K. (2022). Motion detection and classification: Ultra-fast road user detection. *Journal of Big Data*, 9(1), 28.
- OpenCV. (2019). Computer vision annotation tool (cvat) [Accessed 15 August 2022]. <https://github.com/opencv/cvat>
- Poulos, R. G., Hatfield, J., Rissel, C., Grzebieta, R., & McIntosh, A. S. (2012). Exposure-based cycling crash, near miss and injury rates: The safer cycling prospective cohort study protocol. *Injury prevention*, 18(1), e1–e1.
- ppwwyyxx. (2021). Detectron2 model zoo and baselines [Accessed 21 August 2022]. <https://github.com/facebookresearch/detectron2>
- Pucher, J., & Buehler, R. (2016). Safer cycling through improved infrastructure.
- PyTorch. (2022). Multiprocessing package - torch.multiprocessing [Accessed 25 August 2022]. <https://pytorch.org/docs/stable/multiprocessing.html>
- Rick, O. J. C., & Bustad, J. J. (2021). Cycling in the Flattened City: Urban Assemblages and Digital Visual Research [Publisher: Edinburgh University Press]. *Somatechnics*, 11(2), 246–264. <https://doi.org/10.3366/soma.2021.0354>
- Rocky, A., Wu, Q. J., & Zhang, W. (2024). Review of Accident Detection Methods Using Dashcam Videos for Autonomous Driving Vehicles [Conference Name: IEEE Transactions on Intelligent Transportation Systems]. *IEEE Transactions on Intelligent Transportation Systems*, 1–19. <https://doi.org/10.1109/TITS.2024.3354852>
- Snyder, J. P. (1997). *Flattening the earth: Two thousand years of map projections*. University of Chicago Press.
- Taha, M., Zayed, H. H., Nazmy, T., & Khalifa, M. E. (2015). Multi objects tracking in nighttime traffic scenes. *The 7th International Conference on Information Technology*. <https://doi.org/10.15849/icit.2015.0002>
- Tait, C., Beecham, R., Lovelace, R., & Barber, S. (2022). Is cycling infrastructure in london safe and equitable? evidence from the cycling infrastructure database. *Journal of Transport & Health*, 26, 101369.
- timt90022. (2018). Perspective-and-equirectangular [Accessed 20 August 2022]. <https://github.com/timy90022/Perspective-and-Equirectangular>
- Ultralytics. (2020). Yolov5 [Accessed 17 August 2022]. <https://github.com/ultralytics/yolov5>
- Useche, S. A., Alonso, F., Boyko, A., Buyvol, P., Castaneda, I., Cendales, B., Cervantes, A., Echiburu, T., Faus, M., Feitosa, Z., et al. (2022). Cross-culturally approaching the cycling behaviour questionnaire (cbq): Evidence from 19 countries. *Transportation research part F: traffic psychology and behaviour*, 91, 386–400.

- Wang, C., Zhang, W., Feng, Z., Wang, K., & Gao, Y. (2020). Exploring factors influencing the risky cycling behaviors of young cyclists aged 15–24 years: A questionnaire-based study in china. *Risk analysis*, 40(8), 1554–1570.
- Wanner, M., Götschi, T., Martin-Diener, E., Kahlmeier, S., & Martin, B. W. (2012). Active transport, physical activity, and body weight in adults: A systematic review. *American journal of preventive medicine*, 42(5), 493–502.
- Warwickshire Police. (2023). Operation targets motorists who ignore highway code rules by passing cyclists too close. <https://www.warwickshire.police.uk/news/warwickshire/news/2023/september/operation-targets-motorists-who-ignore-highway-code-rules-by-passing-cyclists-too-close/>
- Wojke, N., Bewley, A., & Paulus, D. (2017). Simple online and realtime tracking with a deep association metric. *2017 IEEE international conference on image processing (ICIP)*, 3645–3649.
- Yang, W., Qian, Y., Kämäräinen, J.-K., Cricri, F., & Fan, L. (2018). Object detection in equirectangular panorama. *2018 24th international conference on pattern recognition (icpr)*, 2190–2195.
- Zhang, Y., Xiao, X., & Yang, X. (2017). Real-time object detection for 360-degree panoramic image using cnn. *2017 international conference on virtual reality and visualization (icvr)*, 18–23.
- Zhang, Y., Li, H., & Ren, G. (2023). Analyzing the injury severity in single-bicycle crashes: An application of the ordered forest with some practical guidance. *Accident Analysis & Prevention*, 189, 107126.
- Zhao, Z.-Q., Zheng, P., Xu, S.-t., & Wu, X. (2019). Object detection with deep learning: A review. *IEEE transactions on neural networks and learning systems*, 30(11), 3212–3232.
- Zuraimi, M. A. B., & Zaman, F. H. K. (2021). Vehicle detection and tracking using yolo and deepsort. *2021 IEEE 11th IEEE Symposium on Computer Applications & Industrial Electronics (ISCAIE)*, 23–29.